

# Topological Quantum Computation Algorithms – Day 10

NQIS Summer School

July 19<sup>th</sup> & 23<sup>rd</sup>

1:30—3:30

Eugene Dumitrescu (ORNL)

Assisted by Yan Wang (ORNL)

# Day 10: Topological Aspects of Quantum Algorithms and Computations

- Quantum error correction:
  - Emergent quasiparticles, topological field theories
  - A potential topology underpinning discrete-logic
- Topologies of logical computations
  - Unitary maps (real time evolution), flow field, and fixed points
  - Measurement and imaginary time evolution
- The computation of a dynamical & topological phase transition in a quantum field theory on a quantum computer.

# Topological Field Theories

- Categorical functors (maps on objects) define topological processes. Exchange Statistics is Topological Data

- Types: Particles with various charges

- $\{a_0 \equiv \mathbb{1}, a, b, \dots, z\}$

- Fusion:  $a \times b = \bigoplus_c N_{a,b}^c c = b \times a$

- Anti-particles:  $\forall a \exists \bar{a}$  with fusion

- $a \times \bar{a} = \bigoplus_{c \in \{\mathbb{1}, a, b, \dots\}} N_{a, \bar{a}}^c c = \mathbb{1} + \bigoplus_{c \neq \mathbb{1}} N_{a, \bar{a}}^c c$

- Abelian anyon fusion is deterministic  $a \times b = c$

- Total Quantum Dimension  $\mathcal{D} = \sqrt{\sum_i d_i^2}$

- Abelian anyons  $d_i = 1$

- Non-Abelian anyons  $d_i > 1$

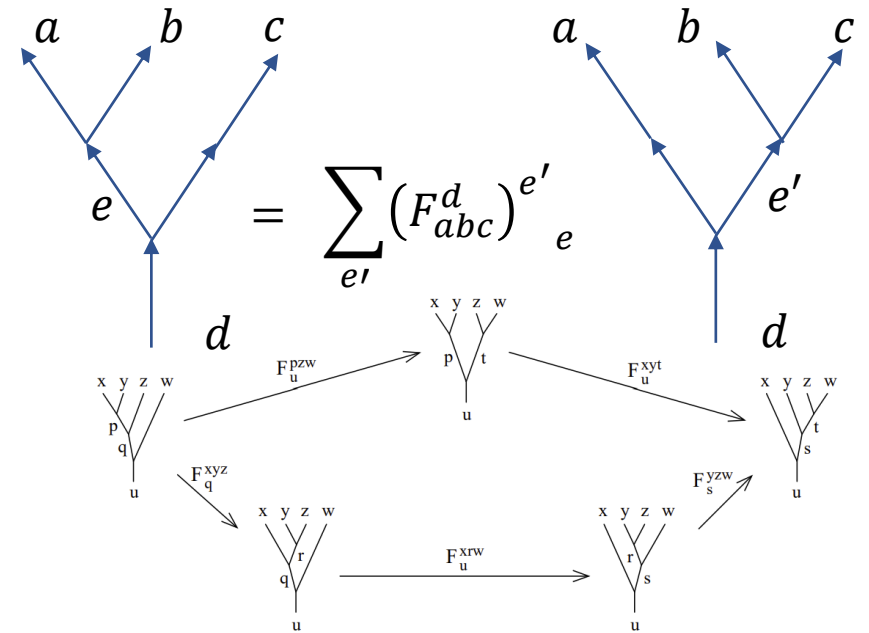
- Birth map:  $\mathbb{1} \rightarrow a \times \bar{a}$  topological degeneracy

- Death map:  $a \times \bar{a} \rightarrow \mathbb{1}$  topological degeneracy

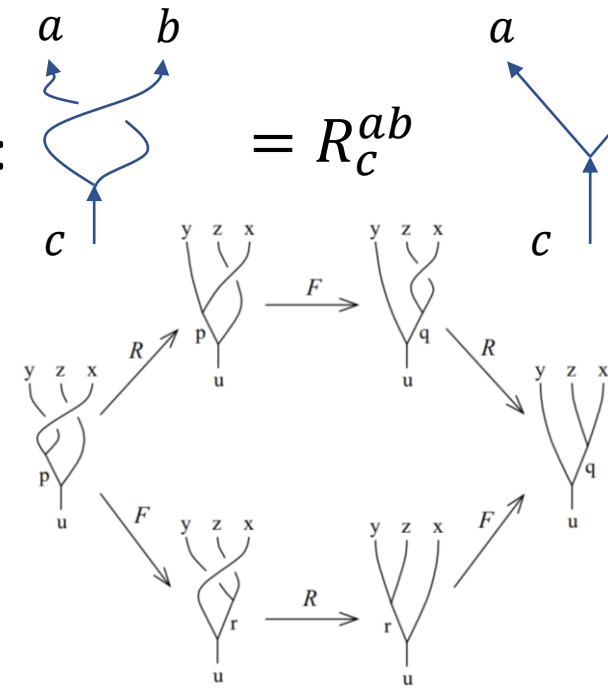
- Intrinsic Internal Topological Twist:

- $\theta_T = \{1, -1, \dots\}$  for bosons, fermions, ...

- F-Matrix: encodes change of basis coefficients



- R matrix:  $= R_c^{ab}$



# Abelian Anyonic Data

- $D(\mathbb{Z}_2)$  or Toric Code :

Simple Obj :  $\{1, e, m, em\}$

Fusion:  $e \otimes e = m \otimes m = em \otimes em = 1, e \otimes m = em, e \otimes em = m, m \otimes em = e$

Quantum Dimension = 1 (for each simple object)

Twists:  $\theta(e^p m^q) = (-1)^{pq}$

- $D(\mathbb{Z}_4)$  or  $\mathbb{Z}_4$  Toric code:

Simple Obj :  $\{1, e, e^2, e^3, m, em, e^2 m, e^3 m, m^2, em^2, e^2 m^2, e^3 m^2, m^3, em^3, e^2 m^3, e^3 m^3\}$

Fusion: similar to Toric code,  $e^a m^b \otimes e^c m^d = e^{a+c \bmod 4} m^{b+d \bmod 4}$

Quantum dimension = 1 (for each simple object)

Twists:  $\theta(e^p m^q) = i^{pq}$

- $D(\mathbb{Z}_N)$  or  $\mathbb{Z}_N$  Toric code:

Simple Obj :  $\{e^a m^b : 0 \leq a, b \leq N-1\}$

Fusion:  $e^a m^b \otimes e^c m^d = e^{a+c \bmod N} m^{b+d \bmod N}$

Quantum dimension = 1 (for each simple object)

Twists:  $\theta(e^p m^q) = e^{2\pi i pq/N}$

- Semion MTC:

Simple Obj :  $\{1, s\}$

Fusion:  $s \otimes s = 1$

Quantum dimension: 1 (for each simple object)

Twists:  $\theta(s) = i$

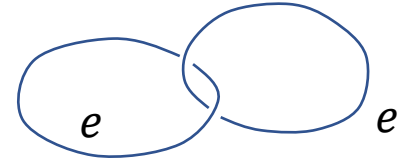
- Doubled Semion MTC:

Simple Obj :  $\{1, s, \bar{s}, s\bar{s}\}$

Fusion:  $s \otimes s = \bar{s} \otimes \bar{s} = s\bar{s} \otimes s\bar{s} = 1, s \otimes \bar{s} = s\bar{s}, s \otimes s\bar{s} = \bar{s}, \bar{s} \otimes s\bar{s} = s$

Quantum dimension: 1 (for each simple object)

Twists:  $\theta(s) = i, \theta(\bar{s}) = -i, \theta(s\bar{s}) = 1$



$$S_{D(\mathbb{Z}_2)} = \frac{1}{2} \begin{pmatrix} 1 & 1 & 1 & 1 \\ 1 & 1 & -1 & -1 \\ 1 & -1 & 1 & -1 \\ 1 & -1 & -1 & 1 \end{pmatrix} \begin{matrix} \mathbb{1} \\ e \\ m \\ em = \epsilon \end{matrix}$$



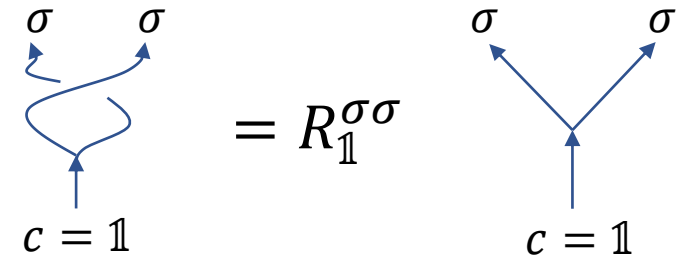
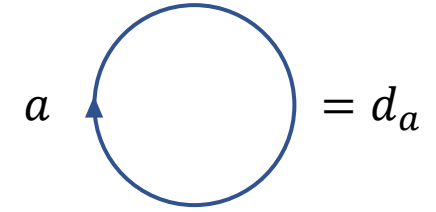
- S-Matrix:  $S^{ab} = \frac{1}{\mathcal{D}} \sum_c d_c \text{Tr}[R_c^{ab} R_c^{ba}]$   
Topological braiding matrix: a non-local scattering process

$$S^{ab} = \mathcal{D}^{-1} \times \text{Diagram}(a, b)$$

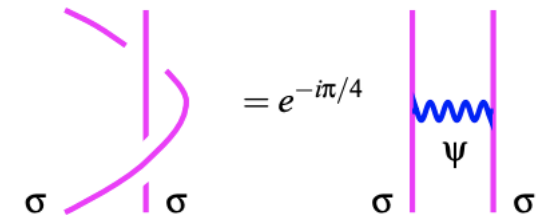
# Ising Modular Tensor Category

- Particles/Simple Objects/Labels:  $\{\mathbb{1}, \sigma, \psi\}$
- Fusion:
  - $\mathbb{1} \times v = v \quad \forall v$
  - $\sigma \times \sigma = \mathbb{1} + \psi$
  - $\sigma \times \psi = \psi \times \sigma = \sigma$
  - $\psi \times \psi = \mathbb{1}$
- Dimensions:
  - $d_{\mathbb{1}} = d_{\psi} = 1; d_{\sigma} = \sqrt{2}$
  - $d(2N \text{ } \sigma \text{ anyons}) = 2^N = d(N \text{ qubits})$ 
    - i.e. N pairs of  $\sigma$
- Topological Twists:
  - $\theta(\mathbb{1}) = 1, \theta(\sigma) = e^{\frac{2\pi i}{16}}, \theta(\psi) = -1$

$$S = \frac{1}{2} \begin{pmatrix} 1 & \sqrt{2} & 1 \\ \sqrt{2} & 0 & \sqrt{2} \\ 1 & \sqrt{2} & -1 \end{pmatrix}$$



R-matrices:  $R_{\mathbb{1}}^{\psi\psi} = -1$   
 $R_{\mathbb{1}}^{\sigma\sigma} = e^{-i\frac{\pi}{8}}, R_{\psi}^{\sigma\sigma} = e^{i\frac{3\pi}{8}}; R_{\sigma}^{\sigma\psi} = R_{\sigma}^{\psi\sigma} = -i$

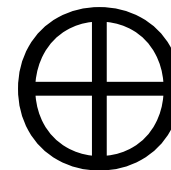
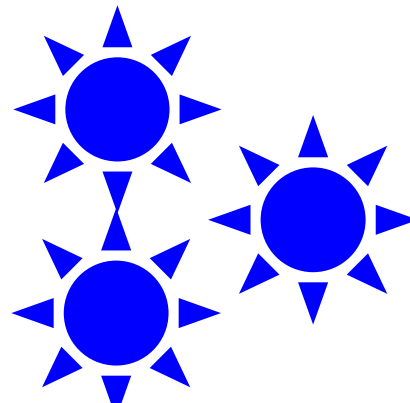
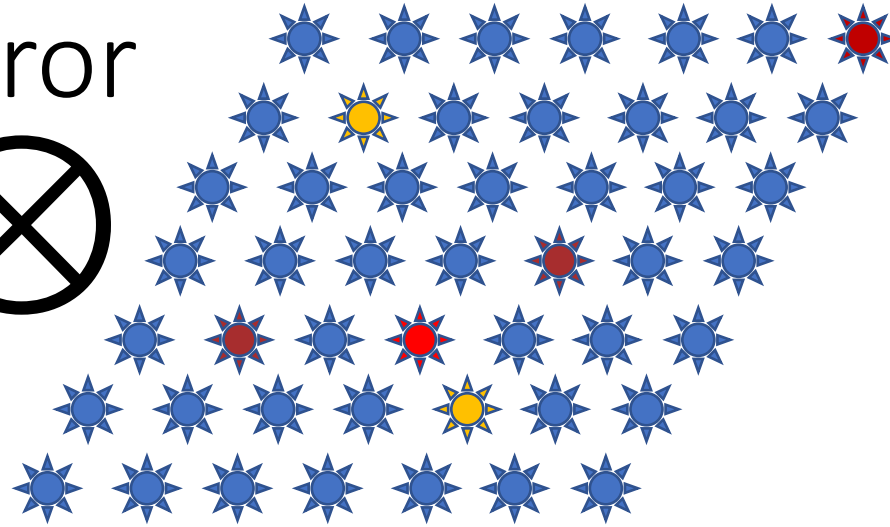
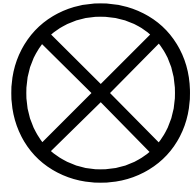


# [[n,k,d]] Quantum Error Correcting Codes

- n – # of *physical* qubits

- d – code *distance*
  - Hamming weight of largest **correctable** error
  - no-cloning theorem constrains distance

- k – # of *logical* qubits



error sectors

E  
N  
C  
O  
D  
E

D  
E  
C  
O  
D  
E

## Quantum Code: A Partitioning

$$\mathcal{S} = \langle \hat{g}_1, \hat{g}_2, \dots, \hat{g}_{n-k} \rangle$$

$$\mathcal{C} = \{ |\psi\rangle \text{ s.t. } g_i |\psi\rangle = |\psi\rangle \forall i \}$$

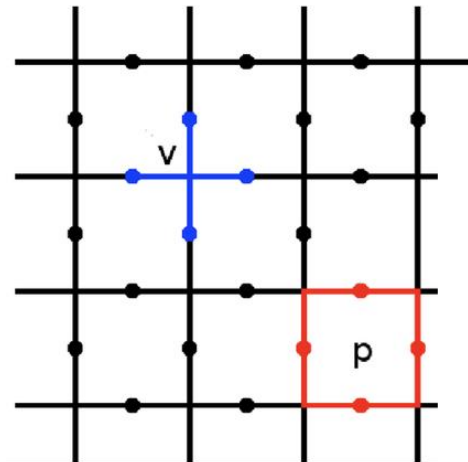
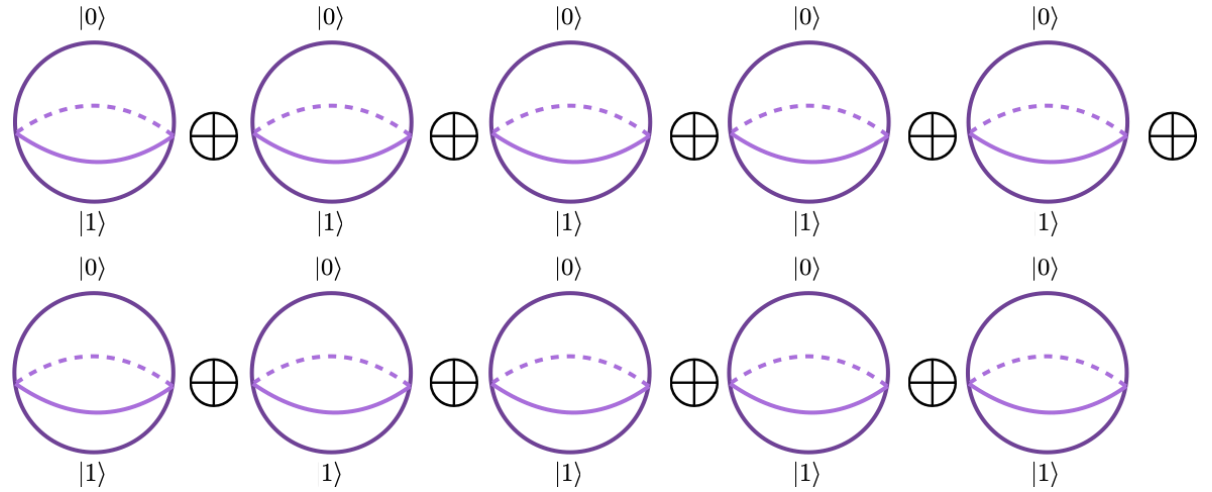
$$\begin{aligned}
 |0\rangle &= |0000000000\rangle + |0011110000\rangle \\
 &\quad + |0101010000\rangle + |0110100000\rangle \\
 &\quad + |1000111111\rangle + |1011001111\rangle \\
 &\quad + |1101101111\rangle + |1110011111\rangle \\
 |1\rangle &= |1111111111\rangle + |1100001111\rangle \\
 &\quad + |1010101111\rangle + |1001011111\rangle \\
 &\quad + |0111000000\rangle + |0100110000\rangle \\
 &\quad + |0010010000\rangle + |0001100000\rangle
 \end{aligned}$$

$\mathcal{C}$

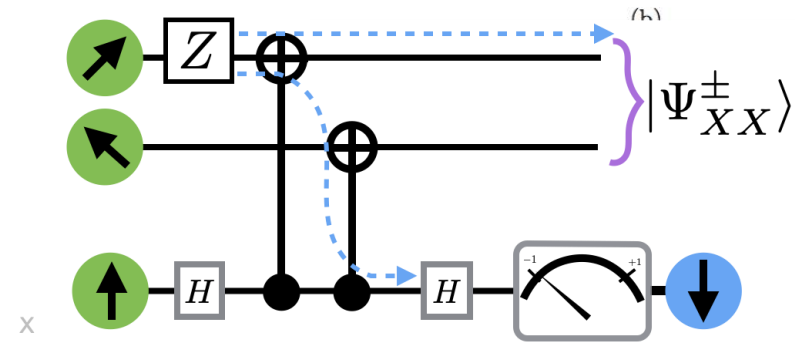
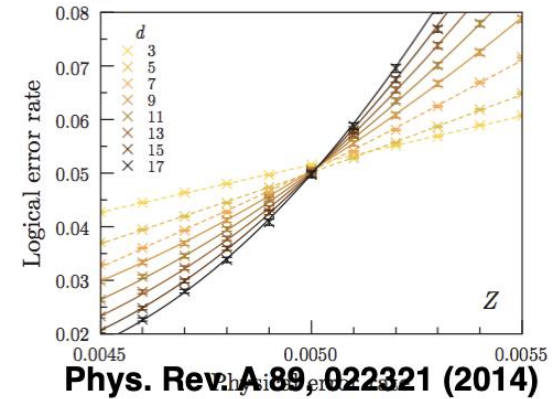
## Quantum Error Correction:

$$\{ \mathbb{E}_i \} \in \mathcal{P}_n = \{ I, X, Y, Z \}^{\otimes n}$$

$$\text{s.t. } \langle \psi_i | \mathbb{E}_a \mathbb{E}_b | \psi_j \rangle = \delta_{ij} \delta_{ab}$$



$$A_v = \prod_{i \in v} \sigma_i^x, \quad B_p = \prod_{i \in p} \sigma_i^z.$$



# Constraints as linear maps

Def: A (stabilizer) constraint  $C_i: \mathcal{H}_i \rightarrow \mathbb{Z}_p$  is a linear mapping from an underlying Hilbert space  $\mathcal{H}_i$  to a measurement result (of dimension  $p$ ).

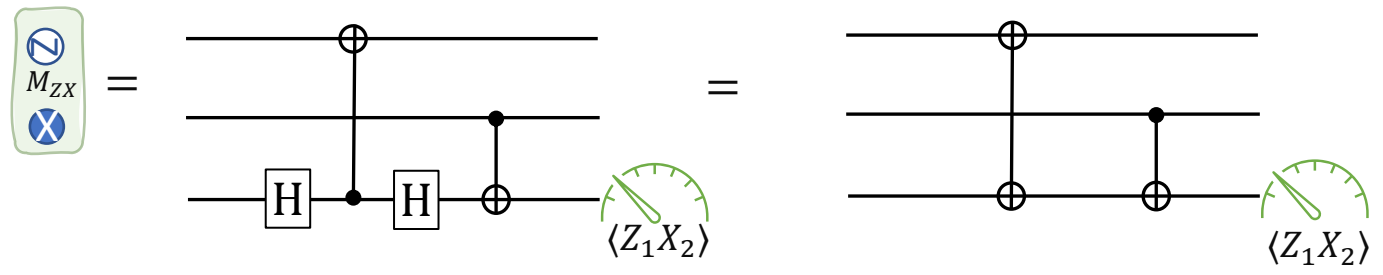
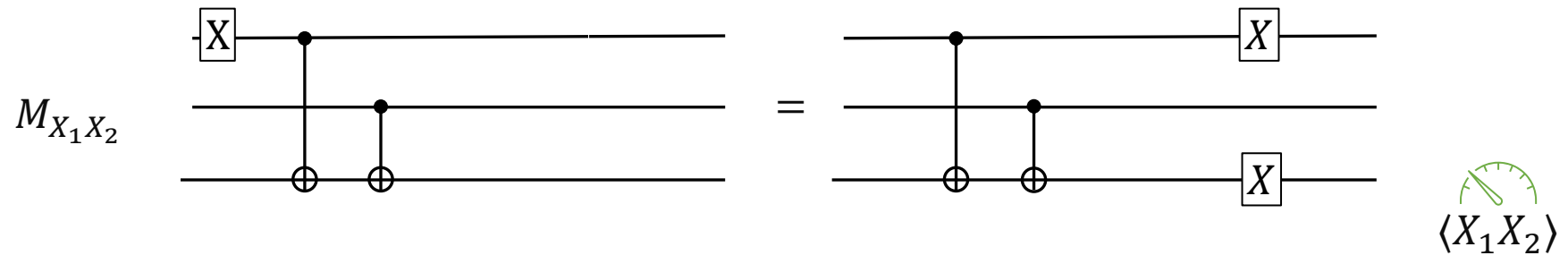
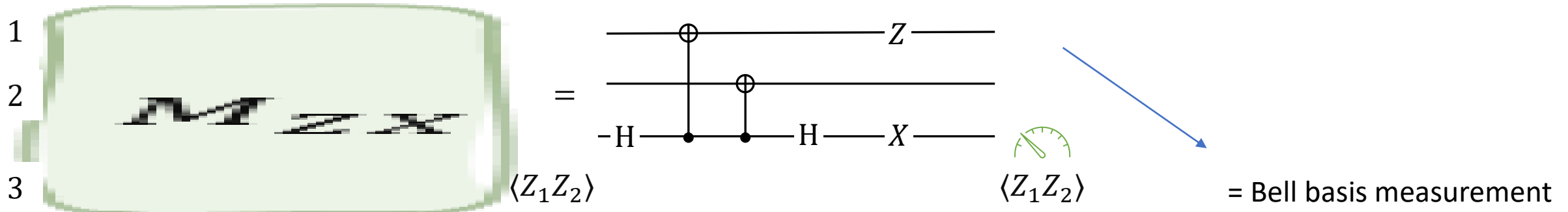
Examples:

A constraint  $C_i := \mathbb{C}^2 \rightarrow \mathbb{Z}_2 = \langle \sigma_i^\mu \rangle = \pm 1$  specifies the  $i^{\text{th}}$  qubit's state.

$$\begin{aligned} Z|i\rangle &= (-1)^i|i\rangle \\ X|\pm\rangle &= \pm|+\rangle = \pm \frac{|0\rangle \pm |1\rangle}{2} \\ Y|\pm i\rangle &= \pm|+\rangle = \pm \frac{|0\rangle \pm i|1\rangle}{2} \end{aligned}$$

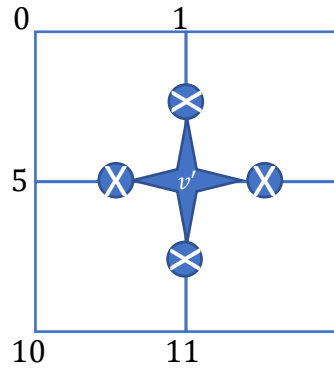
Consider a single two-qubit constraint:  $C_i := \mathbb{C}^2 \otimes \mathbb{C}^2 \rightarrow \mathbb{Z}_2$   
 $\left\langle \sigma_i^{\mu \in \{X,Y,Z\}} \sigma_j^{\nu \in \{X,Y,Z\}} \right\rangle$

# Bell Basis Encoding and Measurement

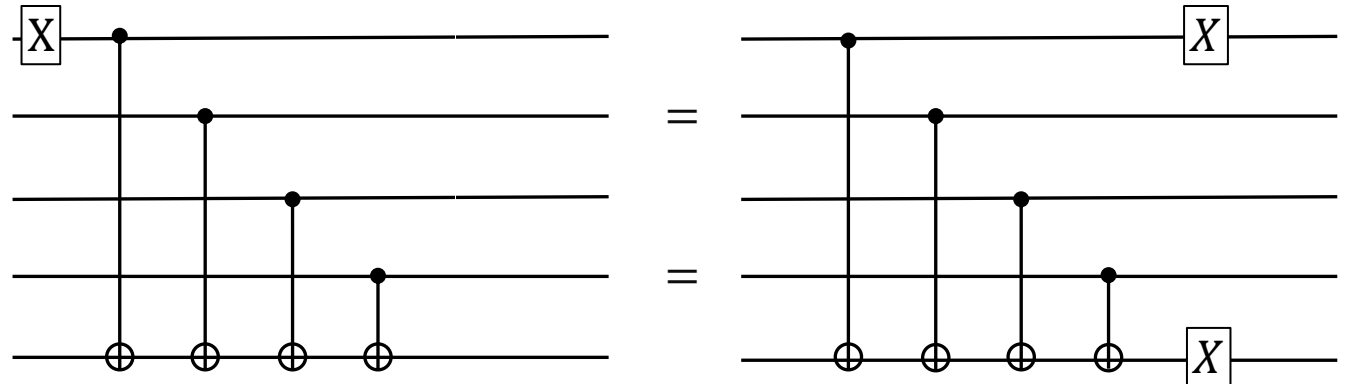


# Eigenvalues of Pauli-product operators

$$\begin{aligned}
 & A_{v,l=k=6} \\
 &= X_{N_V} \otimes X_{E_H} \otimes X_{S_V} \otimes X_{W_H} \\
 &= X_{(k,1)} \otimes X_{(k,7)} \otimes X_{(k,11)} \otimes X_{(k,5)}
 \end{aligned}$$

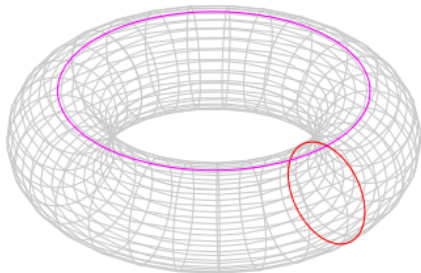


$M_{X_1 X_2}$



$\langle X_1 X_2 \rangle$

$$\begin{aligned}
 B_p &= Z_{N_H} \otimes Z_{E_V} \otimes Z_{S_H} \otimes Z_{W_V} \\
 B_7 &= Z_{(7,8)} \otimes Z_{(8,13)} \otimes Z_{(12,13)} \otimes Z_{(7,12)} \\
 B_p &= Z_i \otimes Z_j \otimes Z_k \otimes Z_l
 \end{aligned}$$



$$\begin{aligned}
 \text{diag}(Z_i) &= \{1, 1, 1, 1, 1, 1, 1, 1, -1, -1, -1, -1, -1, -1, -1, -1\} \\
 \times \text{diag}(Z_j) &= \{1, 1, 1, 1, -1, -1, -1, -1, 1, 1, 1, 1, -1, -1, -1, -1\} \\
 \times \text{diag}(Z_k) &= \{1, 1, -1, -1, 1, 1, -1, -1, 1, 1, -1, -1, 1, 1, -1, -1\} \\
 \times \text{diag}(Z_l) &= \{1, -1, 1, -1, 1, -1, 1, -1, 1, -1, 1, -1, 1, -1, 1, -1\}
 \end{aligned}$$

$$\text{diag}(B_p) = \{1, -1, -1, 1, -1, 1, 1, -1, -1, 1, 1, -1, 1, -1, -1, 1\}$$

$$= \{+1\} \oplus \{-1\}$$

# Toric presentation #1: Electromagnetic lens

- Unit cell coordinates and binary variable index

- Qubits:  $\{i_x, j_y, V \text{ or } H\}$

- V, H considered a unit lattice d.o.f. (sublattice)

- (stabilizers) interaction coordinate:  $\{i_x, j_y, v \text{ or } p\}$

- X-type: if +1 charge **e** vacuum,
  - if -1 charge **e** present

$$A_v = X \otimes X \otimes X \otimes X$$

- Z-type: if +1 flux **m** vacuum,
  - if -1 flux **m** present

$$B_p = Z \otimes Z \otimes Z \otimes Z$$

- By duality  $Z_i$  creates/moves charges. (and  $X_i$  for fluxes)

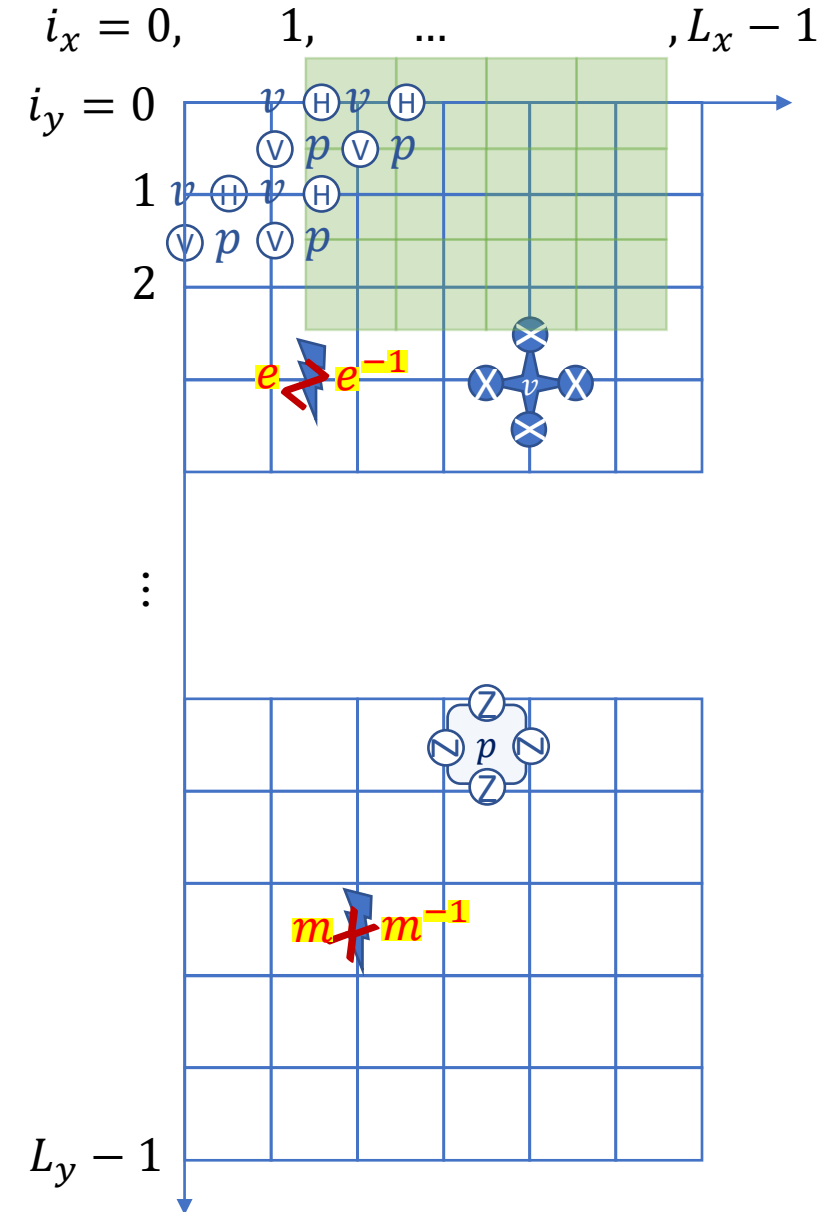
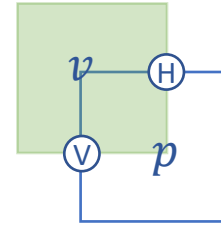
- $H = - \sum_v A_v - \sum_p B_p$

- Particles:

- Charges **e** reside on lattice vertices and move along the edges.
    - Move along the principal lattice; denoted by solid lines
  - Fluxes **m** reside on plaquettes (i.e. dual lattice vertices)
    - Move along the dual lattice; denoted with dashed lines

- $[[\# \text{ of physical qubits}, \# \text{ of logical qubits}, \text{code distance}]] = [[n, k, d]]$

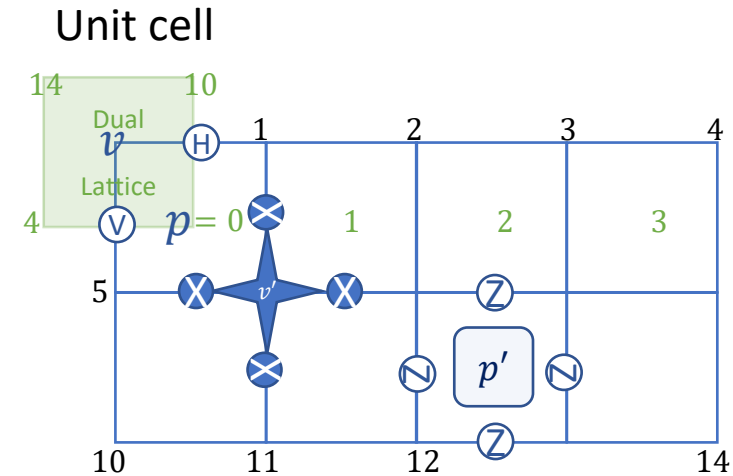
- $[[2N^2, 2, \frac{N}{2} - 1]]$



# Toric presentation #1: Indices Revisited

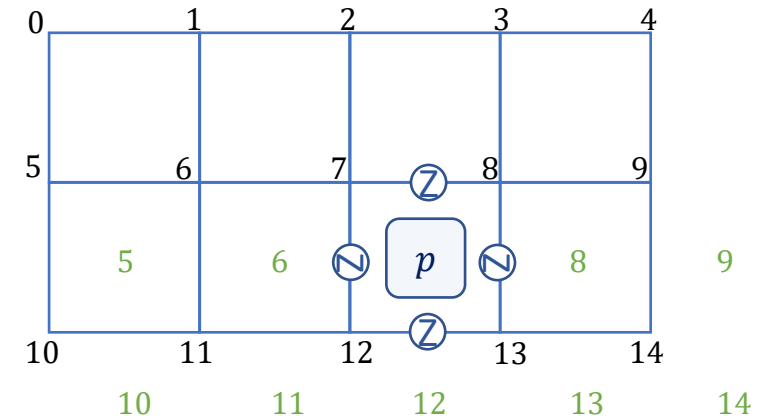
$L_x = 5, L_y = 3$   
(last identified row not illustrated)

- Lattice ( $G = (V, E)$ )
  - Coordinates  $(i_x, j_y) \in (\mathbb{Z}_{L_x}, \mathbb{Z}_{L_y})$
  - Periodic boundaries  $(L_x, j) \equiv (0, j), (i, L_y) \equiv (i, 0)$
- Stabilizers/Interactions/Symmetries coordinate:
  - X-type interaction centered on vertices  $v \in V$ 
    - indexed by coordinates  $(i_x, j_y) \rightarrow k_{xy} = i_x + L_x i_y$
  - Z-type interaction centered on plaquettes  $p$  are centered on the **dual lattice**
- Qubits therefore live on the edges  $E$ 
  - Vertical edges  $E_V \in \{(i, j), (i, j \pm 1)\}$
  - Horizontal edges  $E_H \in \{(i, j), (i \pm 1, j)\}$
  - V, H considered a unit cell (sublattice) degree of freedom



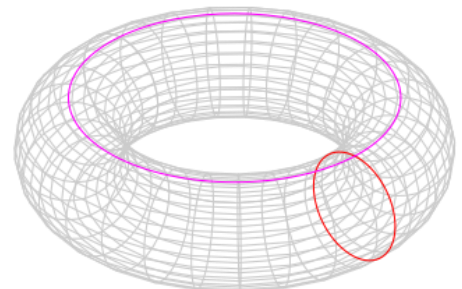
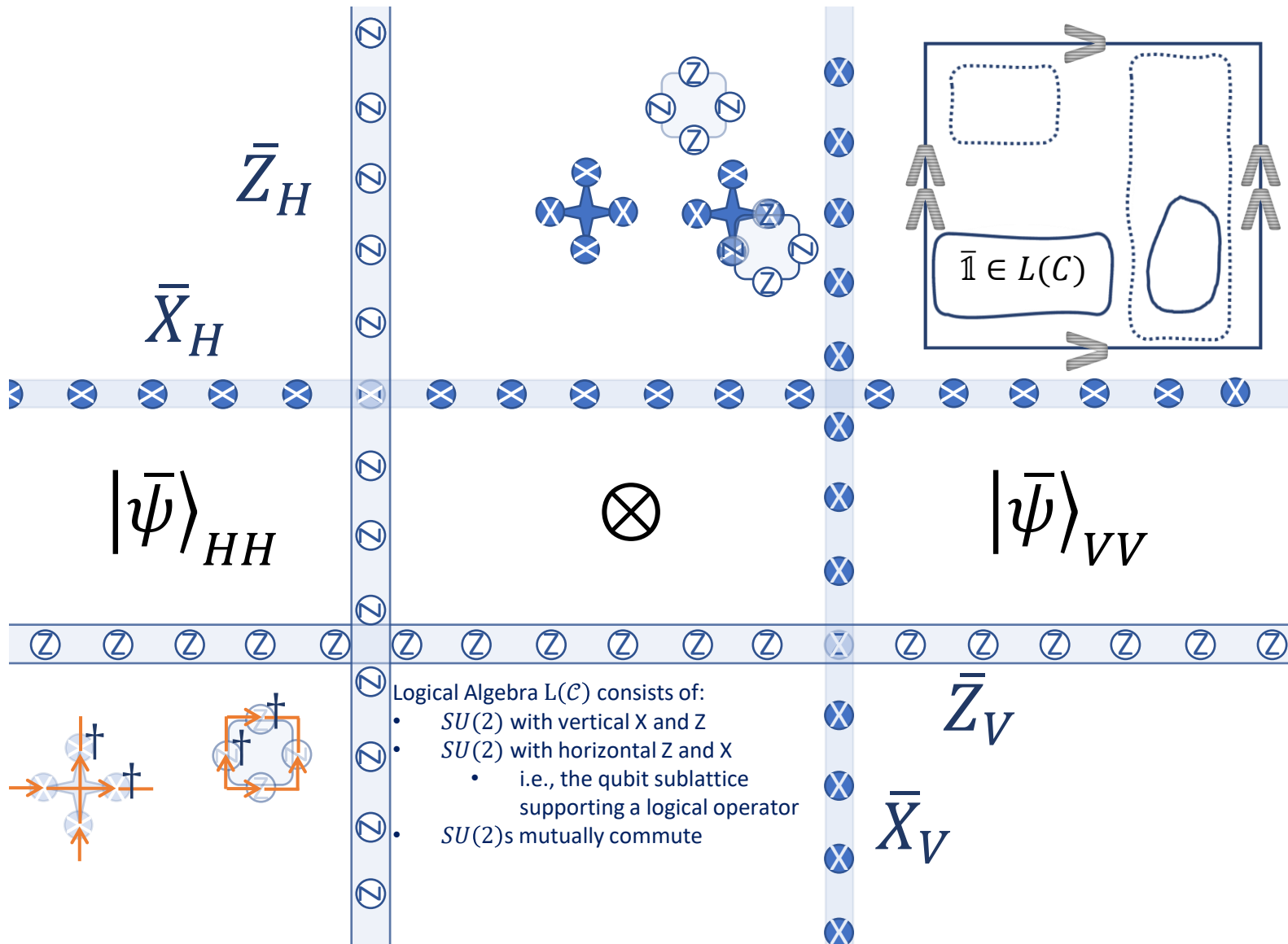
$$A_{v'=k=6} = X_{N_V} \otimes X_{E_H} \otimes X_{S_V} \otimes X_{W_H}$$

$$= X_{(k,1)} \otimes X_{(k,7)} \otimes X_{(k,11)} \otimes X_{(k,5)}$$



$$B_p = Z_{N_H} \otimes Z_{E_V} \otimes Z_{S_H} \otimes Z_{W_V}$$

$$B_7 = Z_{(7,8)} \otimes Z_{(8,13)} \otimes Z_{(12,13)} \otimes Z_{(7,12)}$$



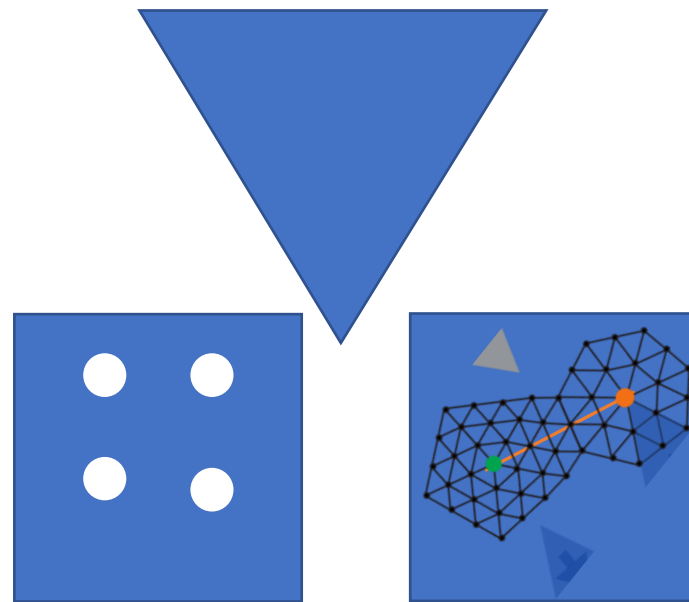
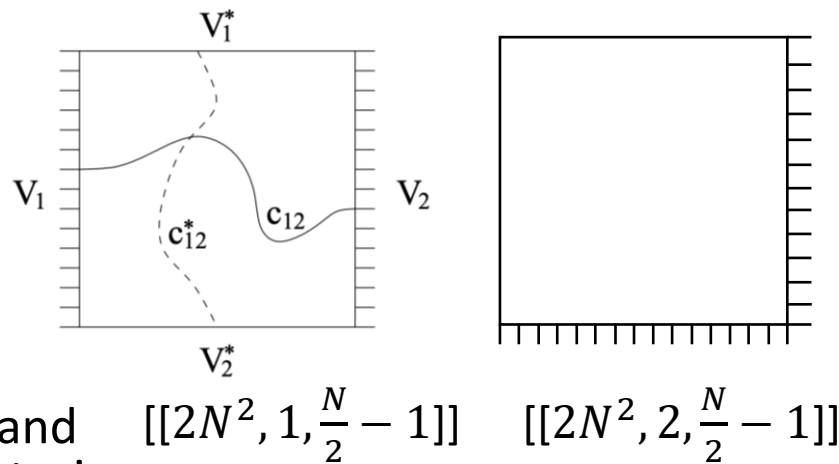
# Unpacking code representations: X-Z and the unit cell(s)

- Boundaries:

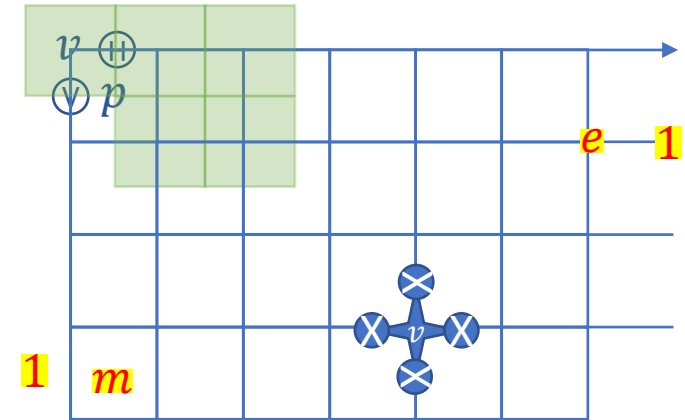
- Rough (x-type)
  - $e \rightarrow 1, m \rightarrow m$
- Smooth (z-type)
  - $e \rightarrow e, m \rightarrow 1$

- Lattice surgeries

- (Dis)connect rough and smooth to (un-)fold toric code
- Reorient rough and smooth for surfaces codes
  - Bravyi, Kitaev 1998
- Multi-genus objects
  - Y-handled torus
  - X punctured surface code
- Twistors
  - Physical (Dehn) twist
  - Algebraic (later) twist

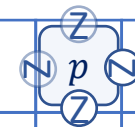


$i_x = 0, \dots, \dots, L_x - 1$



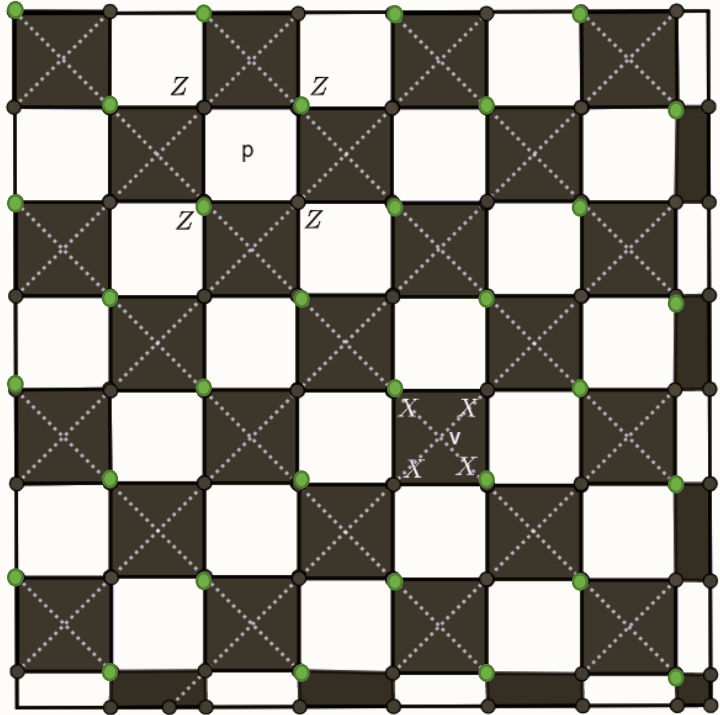
$$A_v = X_{N_H} \otimes X_{E_V} \otimes X_{S_H} \otimes X_{W_V}$$

$$B_p = Z_{N_H} \otimes Z_{E_V} \otimes Z_{S_H} \otimes Z_{W_V}$$



$L_y - 1$

# ZXXZ Presentation: A *symmetrized* Toric Code



1. Rotate lattice by  $\pm \frac{\pi}{4}$

2. Apply  $H^{\otimes \frac{N}{2}}$

Where are the Qubits?

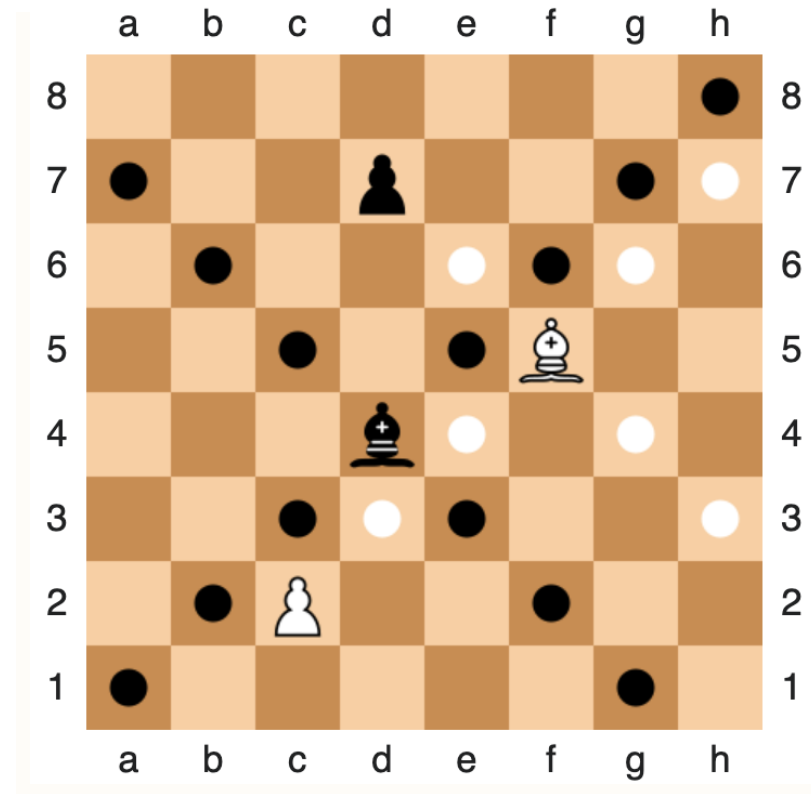
- Previously on edges of dashed lines
- Now on vertices of chessboard lattice

What are the Excitations?

- Charges  $e$ 
  - Previously on lattice *vertices* (dashed lines)
  - Now Black Bishops
- Fluxes  $m$ 
  - Previously on inscribed white plaquettes
  - White Bishops

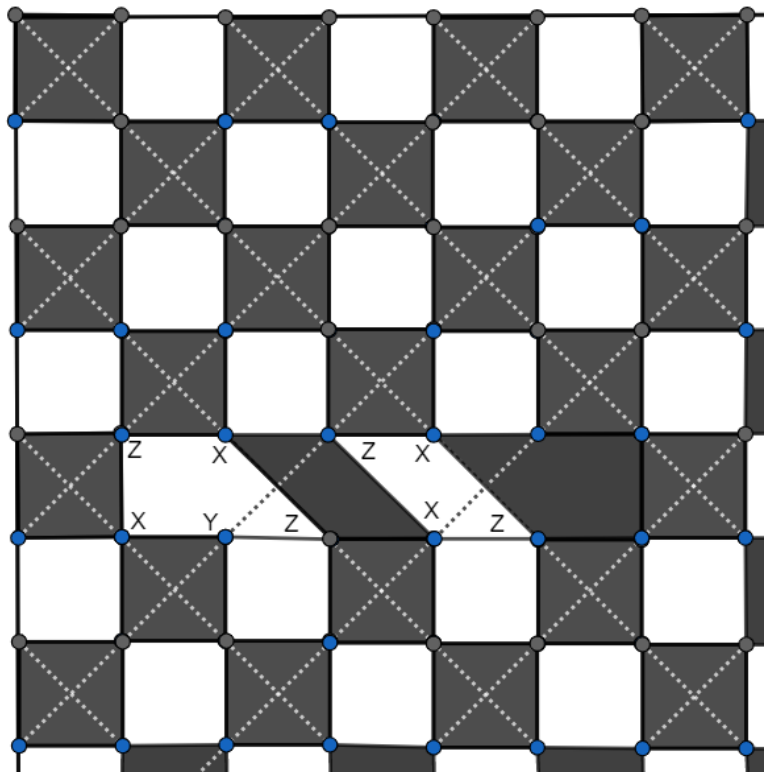
A la Google paper

$$\begin{aligned} (B_r^W, B_{r+\hat{i}}^B) &= \epsilon \\ e \times m &= \epsilon \end{aligned}$$

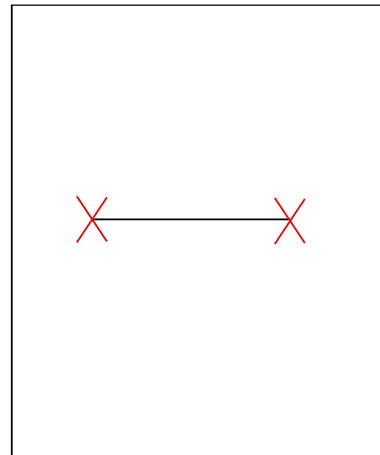


# Algebraic Twist

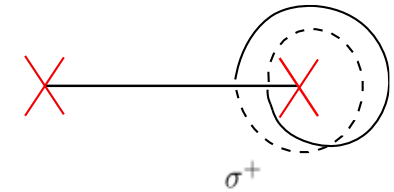
H. Bombin. Topological order with a twist: Ising anyons from an Abelian model. *Physical Review Letters*, 105(3):030403, jul 2010. ISSN 00319007. doi: 10.1103/PhysRevLett.105.030403. URL <https://link.aps.org/doi/10.1103/PhysRevLett.105.030403>.



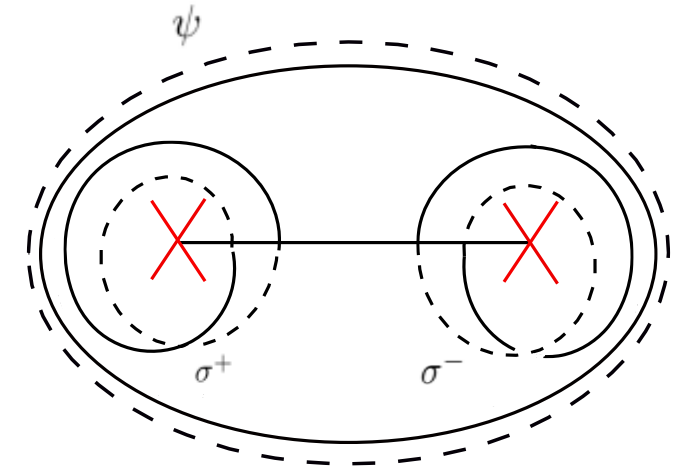
~



$$\psi = em$$



Condensed fermion!  
Chiral logical operators!



The Twist

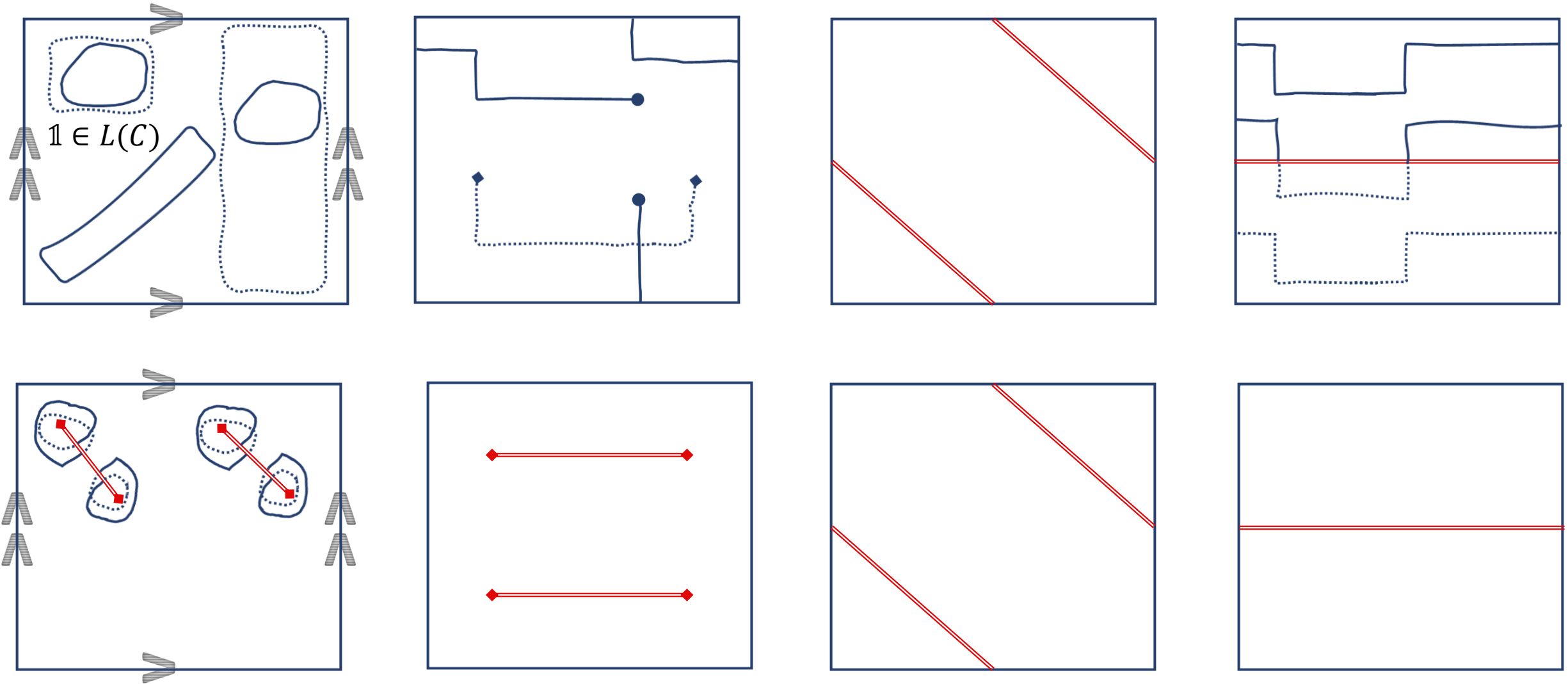
~

Gauging a D=1 defect into D=2 Toric code  
Barkeshli et al 22 arxiv.:2208.07367

# Toric code with a twist(ed qubit)

Deconfined quasiparticles

- Charges hop between vertices via principal lattice
- ❖ Fluxes hop between plaquettes via *dual* (---)lattice



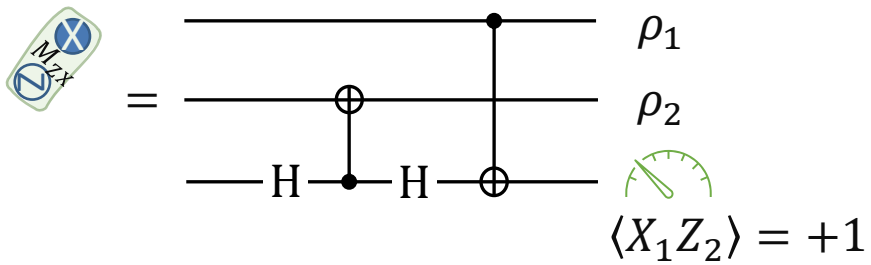
$$S = \left\{ \begin{array}{c} \text{X} \\ \text{X} \text{---} \text{X} \\ \text{X} \end{array} , \begin{array}{c} \text{Z} \\ \text{Z} \text{---} \text{Z} \\ \text{Z} \end{array} , - \begin{array}{c} \text{X} \\ \text{X} \text{---} \text{X} \\ \text{X} \end{array} \begin{array}{c} \text{Y} \\ \text{Z} \text{---} \text{Z} \\ \text{Z} \end{array} \right\}$$

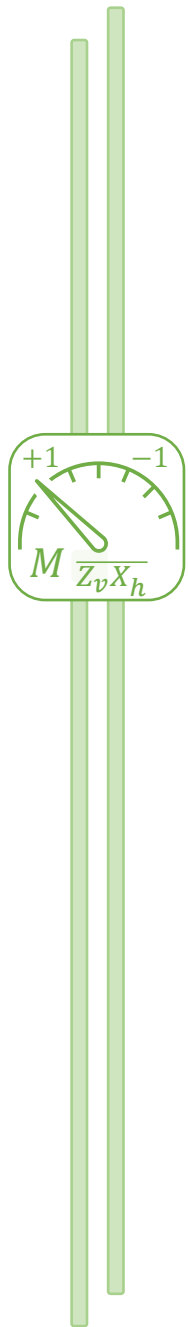
$$S = \{A_v, B_p, A_v B_p\}$$

code deformation via measurement

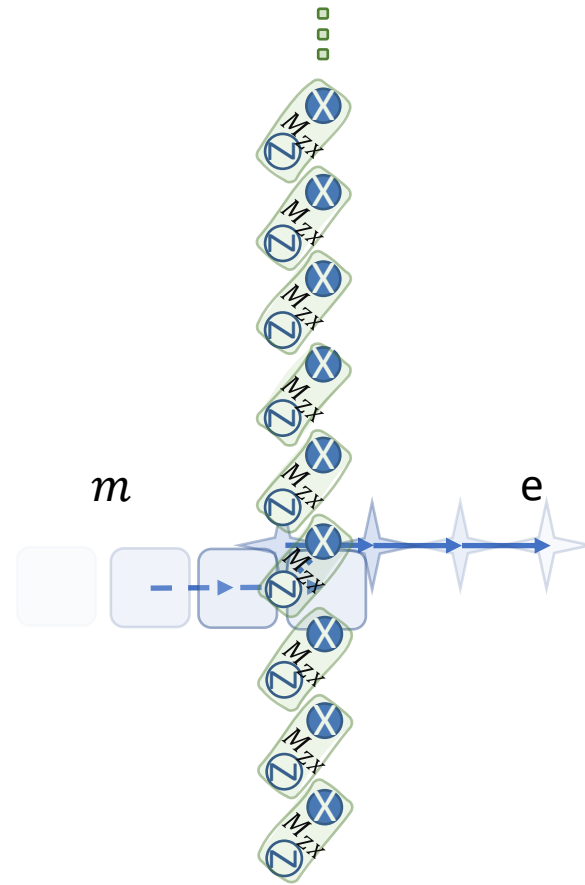
$$S' = \{ZX, A_v B_p, ZX A_v B_p\}$$

$$\rightarrow S' = \left\{ \begin{array}{c} \text{X} \\ \text{Z} \text{---} \text{X} \end{array} , - \begin{array}{c} \text{X} \\ \text{X} \text{---} \text{X} \\ \text{X} \end{array} \begin{array}{c} \text{Y} \\ \text{Z} \text{---} \text{Z} \\ \text{Z} \end{array} , - \begin{array}{c} \text{X} \\ \text{X} \text{---} \text{X} \\ \text{X} \end{array} \begin{array}{c} \text{Z} \\ \text{Z} \text{---} \text{Z} \\ \text{Z} \end{array} \right\}$$



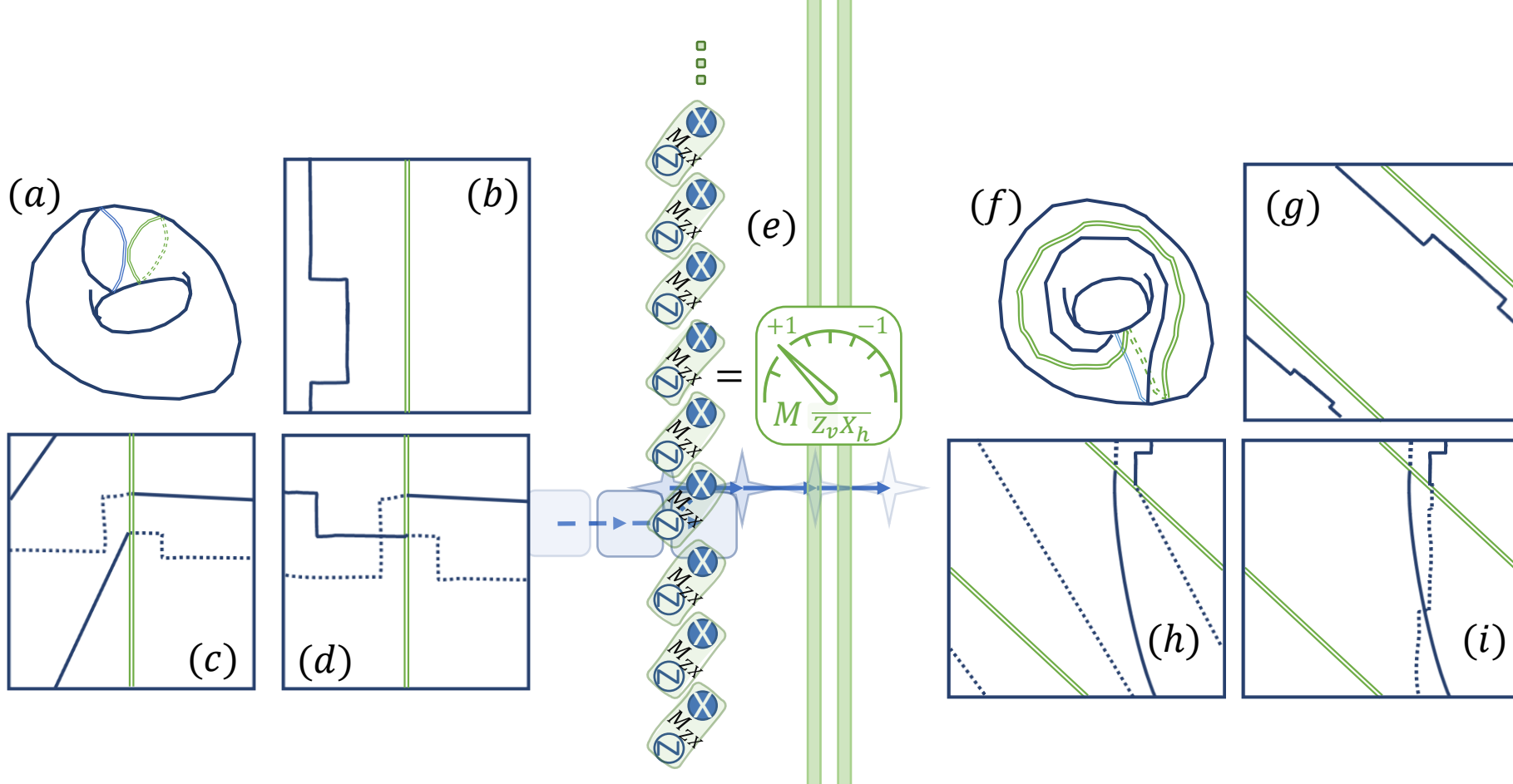


$=$



Zig-zag measurement  $\sim$  a rough-rough boundary functor, condensing  $em = \mathbb{I}$   
 That is,  $e$  and  $m$  annihilate at this internal topological deformation

Anirudh Krishna and David Poulin. *Topological wormholes: Nonlocal defects on the toric code*. Physical Review Research, 2(2), 2020.



*A twisted topological qubit*

$$|\bar{0}\rangle_t \equiv |\bar{0}\rangle_V |\bar{+}\rangle_H$$

$$|\bar{1}\rangle_t \equiv |\bar{1}\rangle_V |\bar{-}\rangle_H$$

$$[[2N^2, \mathbf{1}, \frac{N}{2} - 1]]$$

Distance  $\frac{N}{2} - 1$  for Z errors (b)

$N - 1$  for Y errors (d)

$\frac{3N}{2} - 1$  for X errors (c)

$$S = \{A_v, B_p, A_v B_p\}$$

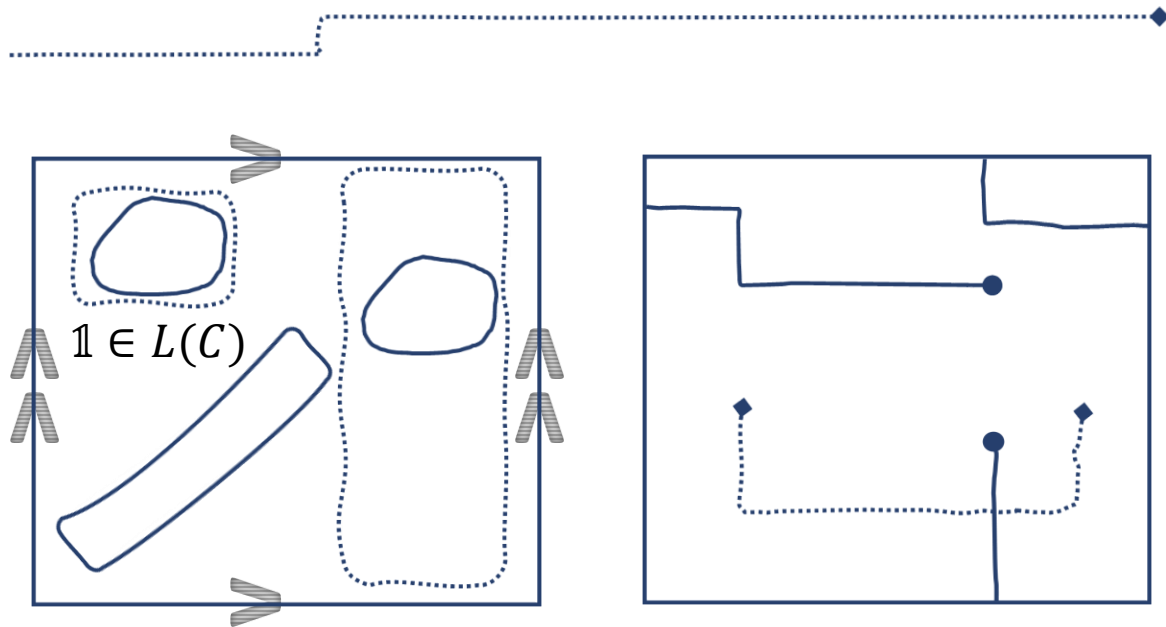
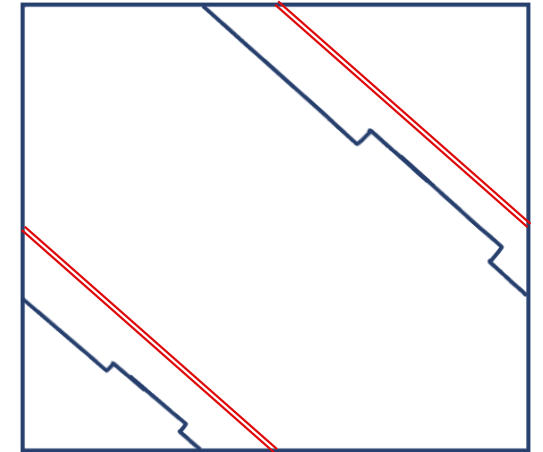
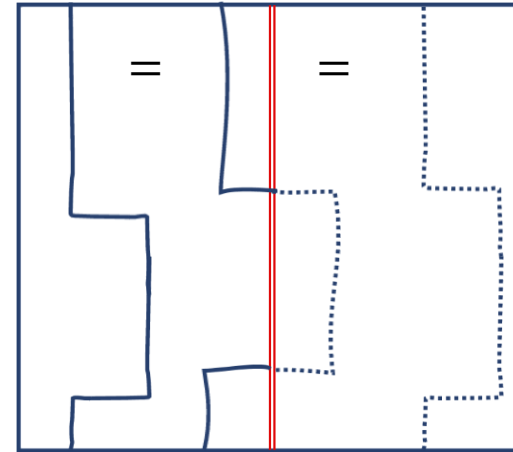


$$S = \{ZX, A_v B_p, ZX A_v B_p\}$$

# Toric code with a twist(ed qubit)

Deconfined quasiparticles include:

- Charges hop between vertices via lattice “streets”
  - Loop action of Z-type
- ❖ Fluxes hop between plaquettes via *dual* lattice
  - ❖ Action of X-type

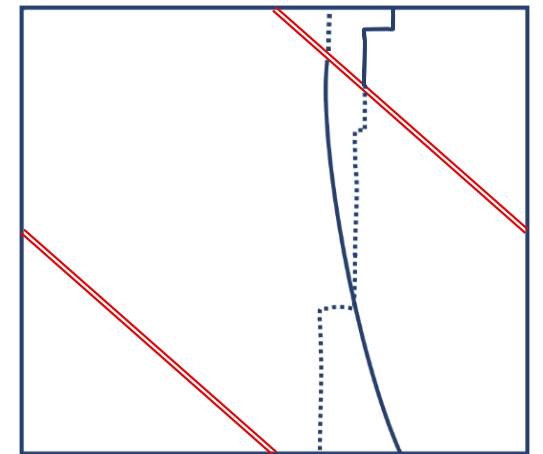
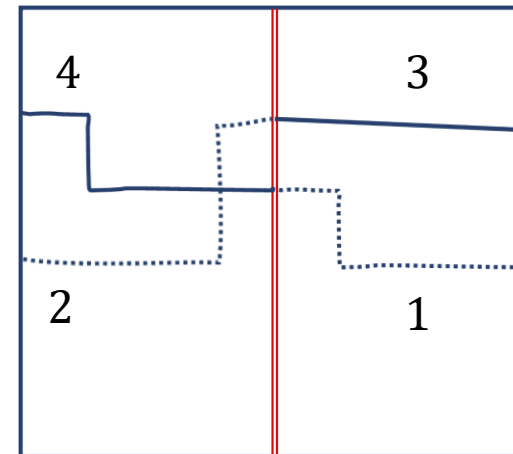


## Logical Operators

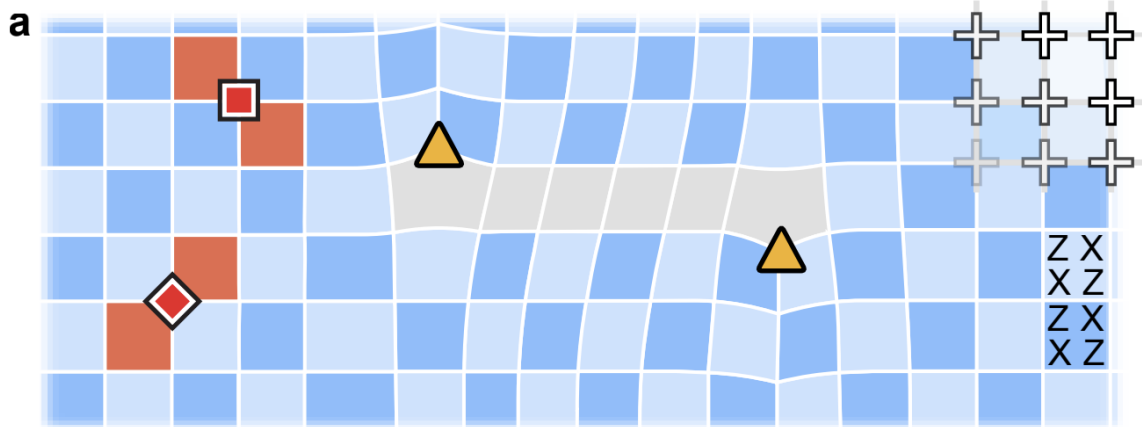
- Logical Z  $\parallel$  to twist
- Logical Y  $\perp$  to twist

$$\bar{X}_{\parallel}^t = \bar{Z}_{\parallel}^t = \sqrt{\bar{X}_{\parallel}^t \bar{Z}_{\parallel}^t} \in \sqrt{\mathbb{1}}$$

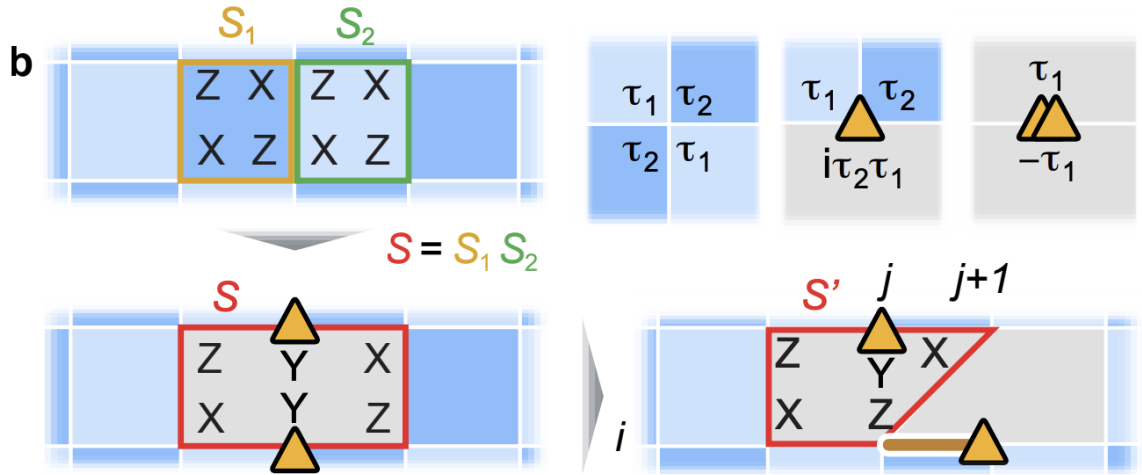
$$\bar{Z}_{\perp}^t \bar{X}_{\perp}^t = +i \bar{Y}_{\perp}^t$$



# Majorana End Twists



◆: Z-gate    ■: X-gate    ▲: D3V



$$U = \exp(\pi/8 [S', S]) = \exp(-i \pi/4 X_{ij} Z_{ij+1})$$

2210.10255 Google Q.AI.

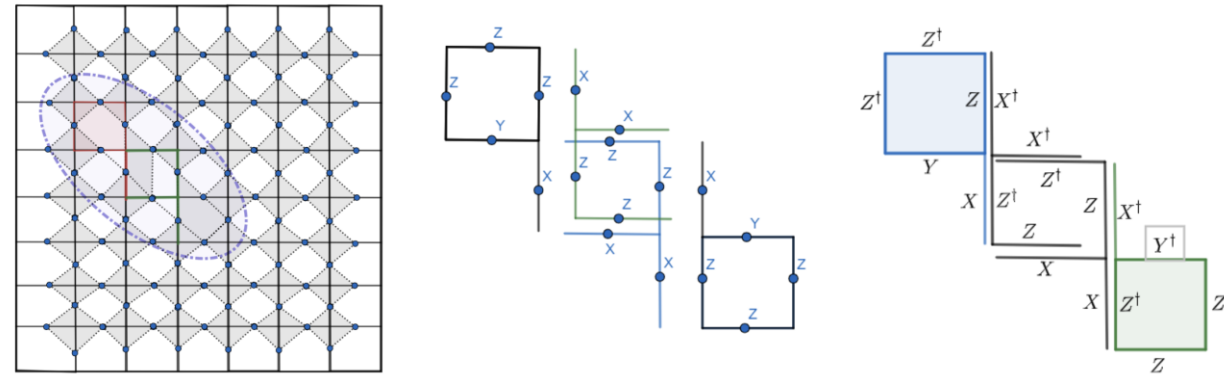


FIG. 10. (i) Embedding Bombin's lattice into Kitaev's, (ii) Twist operators for  $\mathbb{Z}_2$  and (iii)  $\mathbb{Z}_N$

**FIG. 1. Deformations of the surface code.** **a**, Stabilizer codes are conveniently described in a graph framework. Through deformations of the surface code graph, a square grid of qubits (crosses) can be used to realize more generalized graphs. Plaquette violations (red) correspond to stabilizers with  $s_p = -1$  and are created by local Pauli operations. In the absence of deformations, plaquette violations are constrained to move on one of the two sub-lattices of the dual graph in the surface code, hence the two shades of blue. **b**, A pair of D3Vs (yellow triangles) appears by removing an edge between two neighboring stabilizers,  $\hat{S}_1$  and  $\hat{S}_2$ , and introducing the new stabilizer,  $\hat{S} = \hat{S}_1 \hat{S}_2$ . A D3V is moved by applying a 2-qubit entangling gate,  $\exp\left(\frac{\pi}{8} [\hat{S}', \hat{S}]\right)$ . In the presence of bulk D3Vs, there is no consistent way of checkerboard coloring, hence the (arbitrarily chosen) gray regions. Top right: in a general stabilizer graph,  $\hat{S}_p$  can be found from a constraint at each vertex, where  $\{\tau_1, \tau_2\} = 0$ .

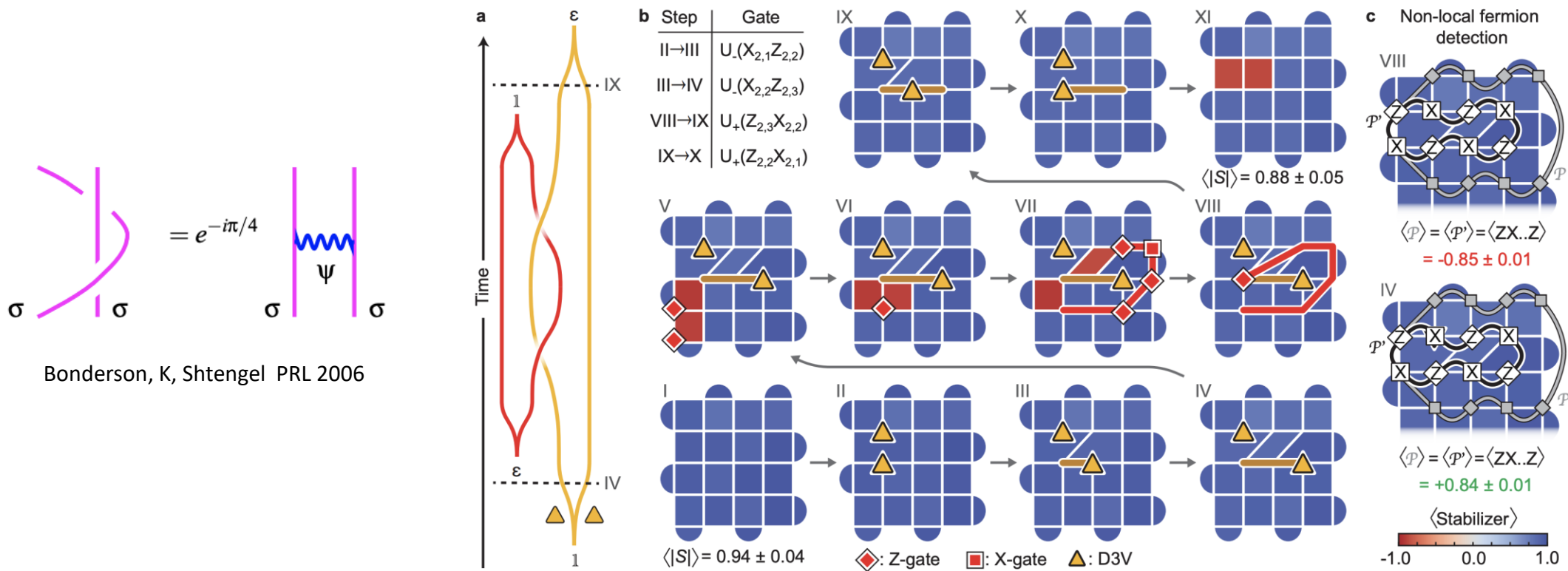
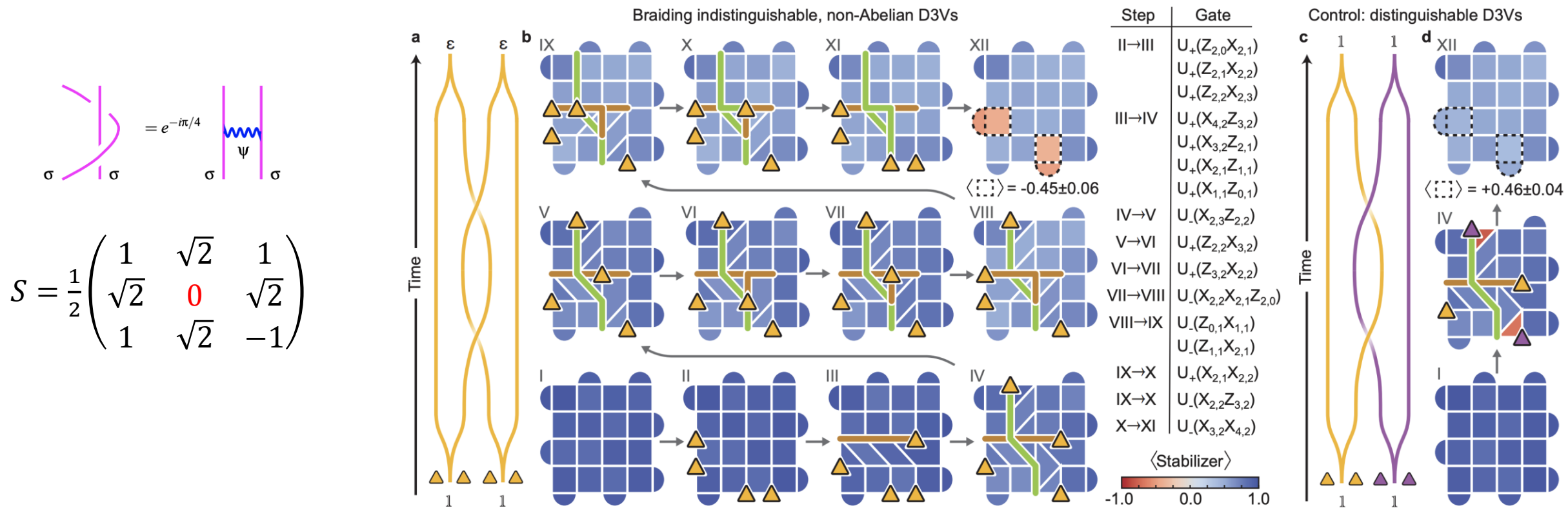


FIG. 2. **Demonstration of the fundamental fusion rules of D3Vs.** **a**, The braiding worldlines used to fuse  $\varepsilon$  and  $\sigma$ . **b**, Expectation values of stabilizers at each step of the unitary operation after readout correction (see Fig. S3 for details and individual stabilizer values). We first prepare the ground state of the surface code (step I; average stabilizer value:  $0.94 \pm 0.04$ ). A D3V ( $\sigma$ ) pair is then created (II) and separated (III-IV), before creating a fermion,  $\varepsilon$  (V). One of the plaquette violations is brought around the right  $\sigma$  (VI-VIII), allowing it to annihilate with the other plaquette violation (VIII). The fermion has seemingly disappeared, but re-emerges when the  $\sigma$  are annihilated (XI; stabilizer values:  $-0.86$  and  $-0.87$ ). The path V→VIII demonstrates the fusion rule,  $\sigma \times \varepsilon = \sigma$ . The different fermion parities at the end of the paths VIII→XI and IV→I show the other fusion rule,  $\sigma \times \sigma = \mathbb{1} + \varepsilon$ . Yellow triangles represent the positions of the  $\sigma$ . The brown and red lines denote the paths of the  $\sigma$  and the plaquette violation, respectively. Red squares (diamonds) represent X- (Z-) gates. Upper left: table of two-qubit unitaries used in the protocol. **c**, Non-local technique for hidden fermion detection: the presence of a fermion in a  $\sigma$ -pair can be deduced by measuring the sign of the Pauli string  $\hat{P}$  corresponding to bringing a plaquette violation around the  $\sigma$ -pair (gray path).  $\hat{P}$  is equivalent to the shorter string  $\hat{P}'$  (black path). Measurements of  $\hat{P}'$  in steps VIII (top) and IV (bottom) give values  $-0.85 \pm 0.01$  and  $+0.84 \pm 0.01$ , respectively. This indicates that there is a hidden fermion pair in the former case, but not in the latter, despite the stabilizers being the same.



**FIG. 3. Braiding of non-Abelian anyons.** **a**, Wordline schematic of the braiding process. **b**, Experimental demonstration of braiding, displaying the values of the stabilizers throughout the process. Two  $\sigma$ -pairs, A and B, are created from the vacuum  $\mathbb{1}$ , and one of the  $\sigma$  in pair A is brought to the right side of the grid. Next, a  $\sigma$  from pair B is moved to the top, thus crossing the path of pair A, before bringing  $\sigma$ -pairs A and B back together to complete the braid. In the final step, two fermions appear in the locations where the  $\sigma$ -pairs resided, constituting a change in the local observables. The diagonal  $\sigma$  move in step IV requires two SWAP-gates (3 CZ-gates each) and a total of 10 CZ-gates. The three-qubit unitary in step VIII requires 4 SWAP-gates and a total of 15 CZ-gates. In the full circuit, a total of 40 layers of CZ-gates are applied (see Supplementary materials). The yellow triangles represent the locations of the  $\sigma$ ; the brown and green lines represent the paths of  $\sigma$  from pair A and B, respectively. **c**, As a control experiment, we perform the same braid as in **a**, but with distinguishable  $\sigma$  by attaching a plaquette violation to the  $\sigma$  in pair B (represented as purple triangles). **d**, Same as **b**, but using distinguishable  $\sigma$  (only showing steps I, IV and XII). In contrast to **b**, no fermions are observed in step XII.

2210.10255

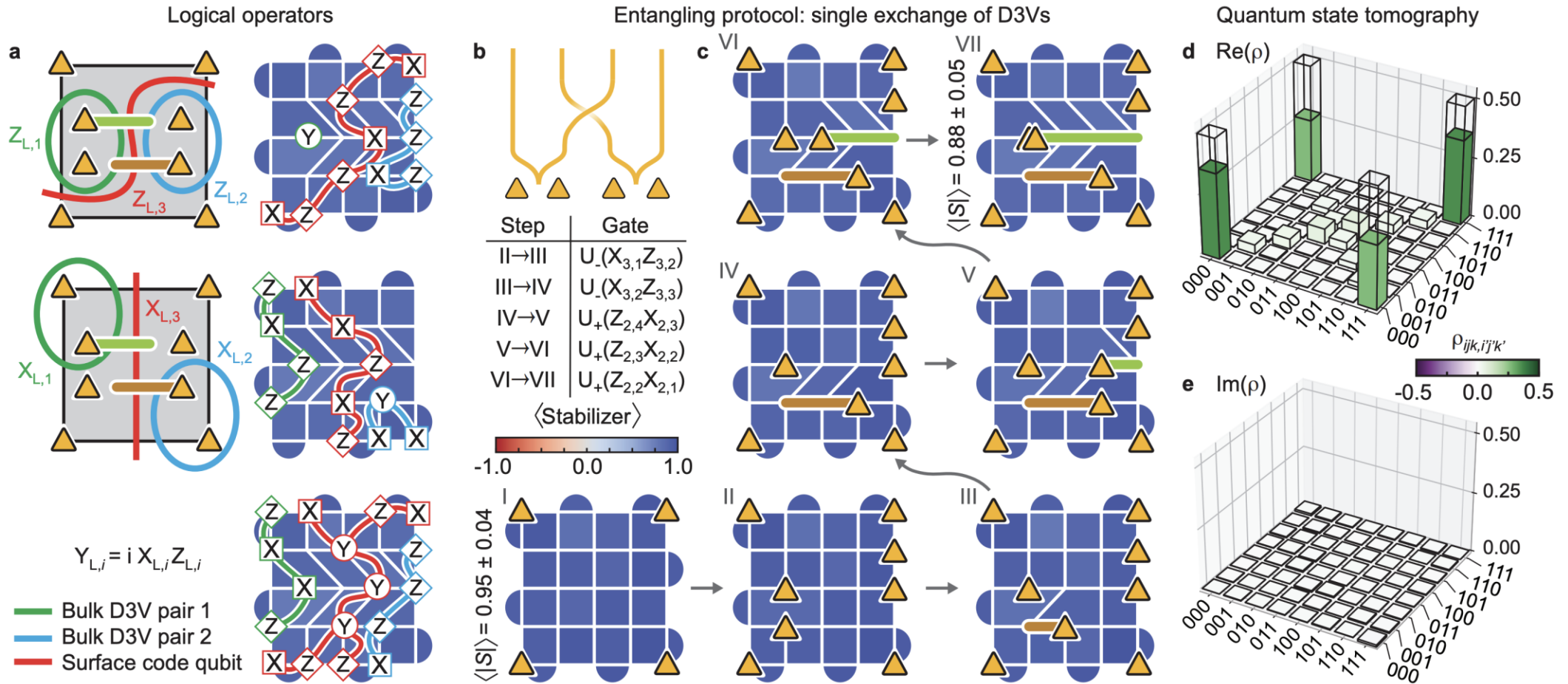


FIG. 4. **Entangled state of anyon-encoded logical qubits via braiding.** **a**, Logical operators of the three logical qubits encoded in the 8 anyons (other basis choices are possible). The colored curves in the left column denote plaquette violation paths, before reduction to shorter, equivalent Pauli strings measured in the experiment (right column). **b**, Worldline schematic of the single exchange used to realize an entangled state of the logical qubits. **c**, Single exchange of the non-Abelian anyons, displaying measurements of the stabilizers throughout the protocol. Yellow triangles represent the locations of the  $\sigma$ , while brown and green lines denote their paths. The average absolute stabilizer values are  $0.95 \pm 0.04$  and  $0.88 \pm 0.05$  in the first and last step, respectively. **d,e**, Real (**d**) and imaginary (**e**) parts of the reconstructed density matrix from the quantum state tomography.  $\text{Re}(\rho)$  has clear peaks in its corners, as expected for a GHZ state on the form  $(|000\rangle + |111\rangle)/\sqrt{2}$ . The overlap with the ideal GHZ-state is  $\text{Tr}\{\rho_{\text{GHZ}}\rho\} = 0.623 \pm 0.004$ .

# Topology of dynamics: (complex) time-evolution

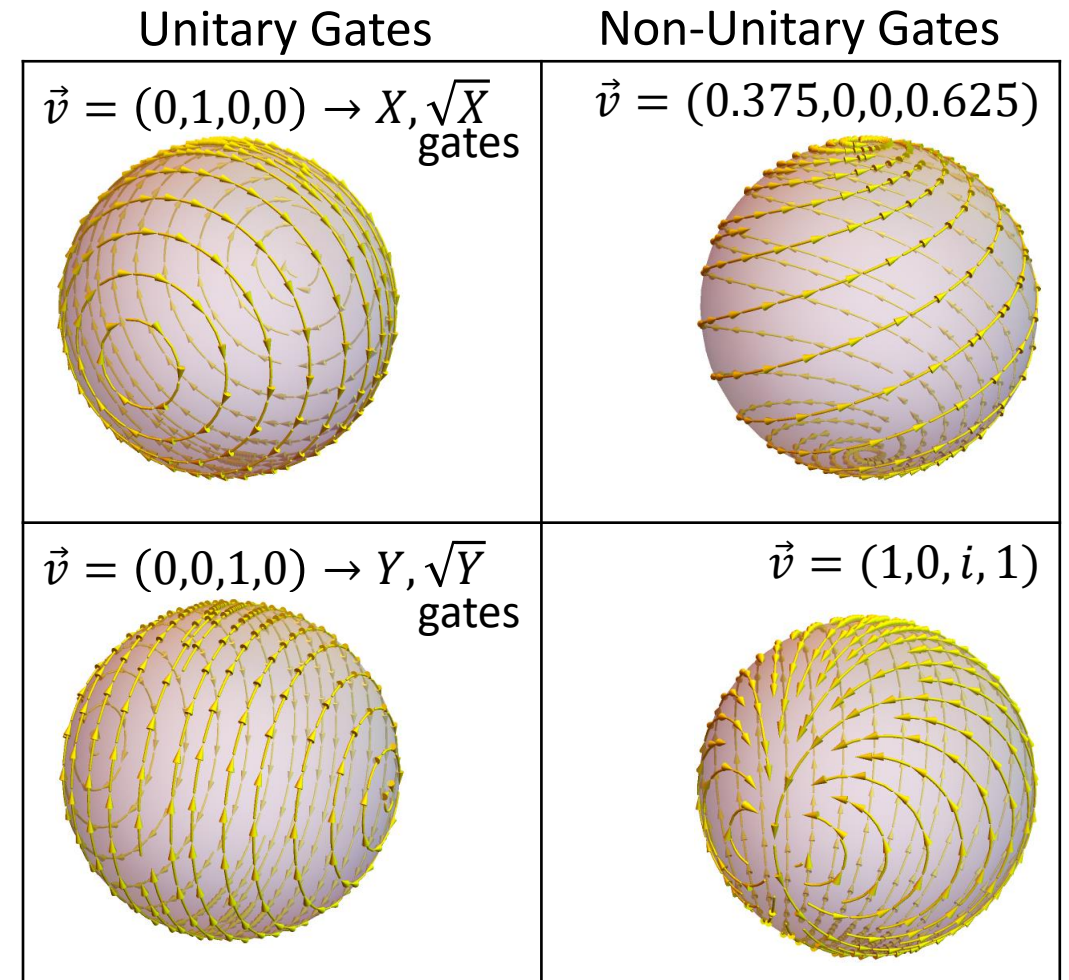
- State's rate of change defines field lines in Hilbert space.
  - $|\Psi\rangle$  was a vector, so is  $|\dot{\Psi}\rangle = \partial_t |\Psi\rangle = \frac{\partial}{\partial t} |\Psi\rangle = \frac{-i}{\hbar} H(t) |\Psi\rangle$
  - For (real-time evolution) Unitary operator (in spectral basis):
    - Field lines *orbit* the eigenstates (which are fixed points)
  - For Imaginary-Time evolution operators or Measurement gates
    - Field lines flow *towards* measurement basis (which are fixed points)
- Dynamical Quantum Phase Transition
  - Brief technical encoding of problem
  - Fermionic topological invariants encoded in topology of dynamical manifold
    - momentum-frequency  $(k, \omega)$  space
    - Topological invariant is the number of poles in the manifold defined by the dynamical quantum Green's (a.k.a. propagation or correlation) function
    - Diagonalization of free-theory and experiment
  - Calculation of topo invariant
    - Take home assignment, do this for 2, 4 lattice sites (4, 8 qubits)

# Unitary vs Non-Unitary Time Evolution

-- example with one-qubit  $SU(2, \mathbb{C})$  "gates"

- $SU(2)$  basis:  $X, Y, Z, I$
- Generators:  $G = v_0 I + v_1 X + v_2 Y + v_3 Z, \vec{v} \in \mathbb{C}^4$
- Time ( $t$ ) evolution operator generated by  $G: e^{-itG}$ 
  - Unitary:  $\vec{v} \in \mathbb{R}^4$
  - Non-unitary:  $\vec{v} \in \mathbb{C}^4 \setminus \mathbb{R}^4$
- Non-unitary  $\rightarrow$  unitary (measurement postulate):  
Valid Quantum Map on  $\rho = |\psi\rangle\langle\psi|$

$$\frac{e^{-itG} \rho e^{itG^\dagger}}{\text{Tr}(e^{-it(G-G^\dagger)} \rho)}$$



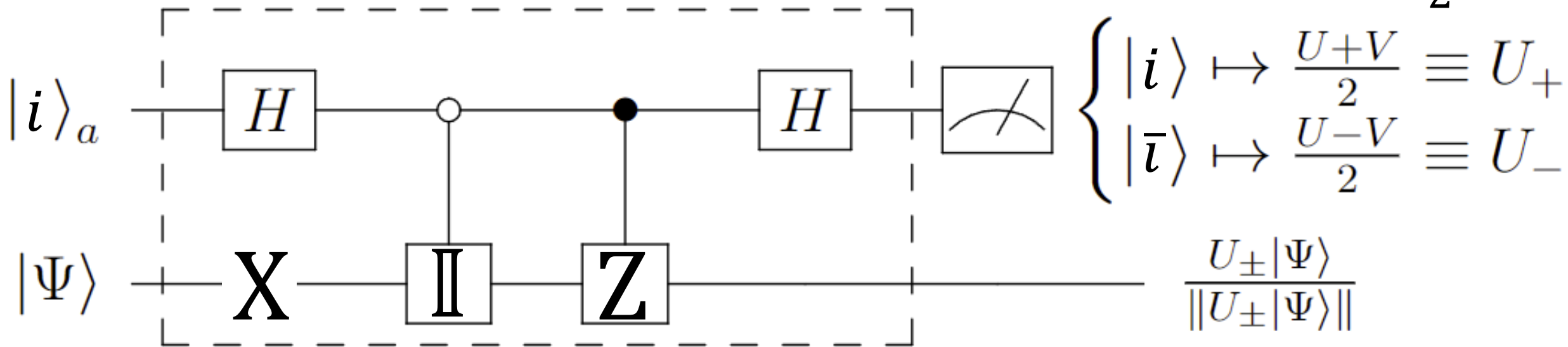
**Orbits of unitary gates vs non-unitary gates**

(see also: A. Galda and V.M. Vinokur, "Linear dynamics of classical spin as Möbius transformation," Sci. Rep. **7**, 1168 (2017).)

# The Only Quantum Circuit You'll Ever Need

$$\overleftarrow{X \cdot (\mathbb{I} \mp Z) = X \pm iY = (\mathbb{I} \pm Z) \cdot X}$$

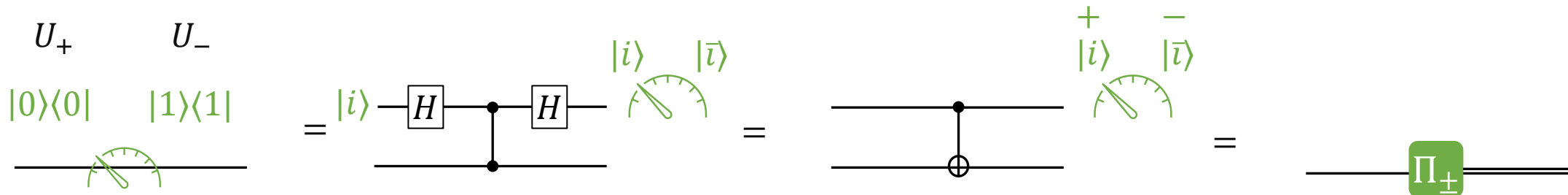
$$\frac{\mathbb{I} \pm Z}{2}$$



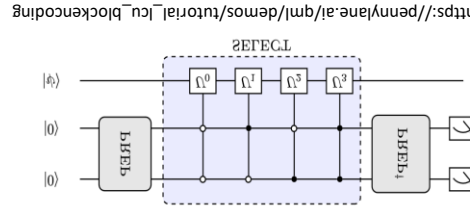
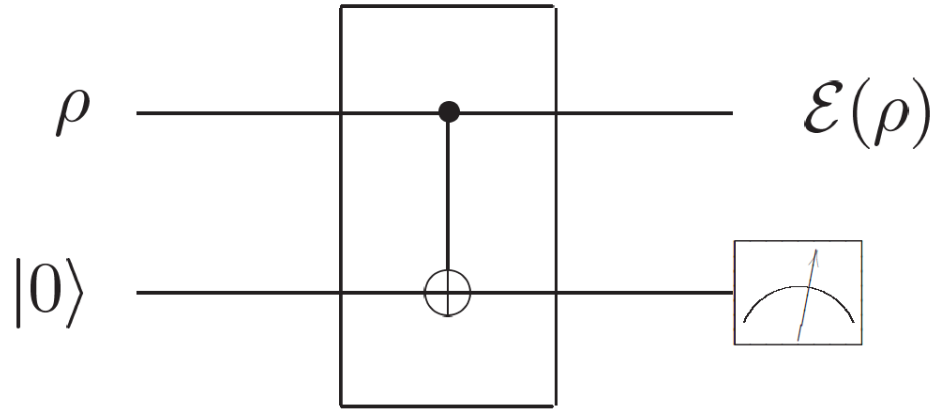
time

Note the state-dependent weighting factors

$$\|U_i |\Psi\rangle\|$$



Mike & Ike, Chapter pp362



LCU of  $\frac{I}{2} \pm \frac{Z}{2}$

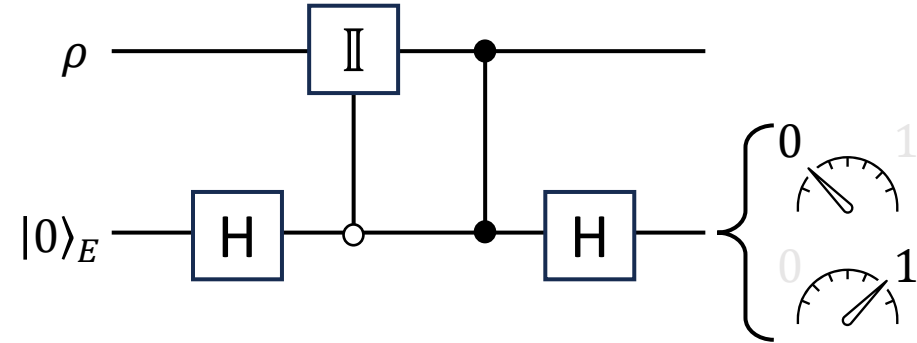


Figure 8.5. Controlled-NOT gate as an elementary model of single qubit measurement.

$$U = |0_P 0_E\rangle\langle 0_P 0_E| + |0_P 1_E\rangle\langle 0_P 1_E| + |1_P 1_E\rangle\langle 1_P 0_E| + |1_P 0_E\rangle\langle 1_P 1_E|. \quad (8.24)$$

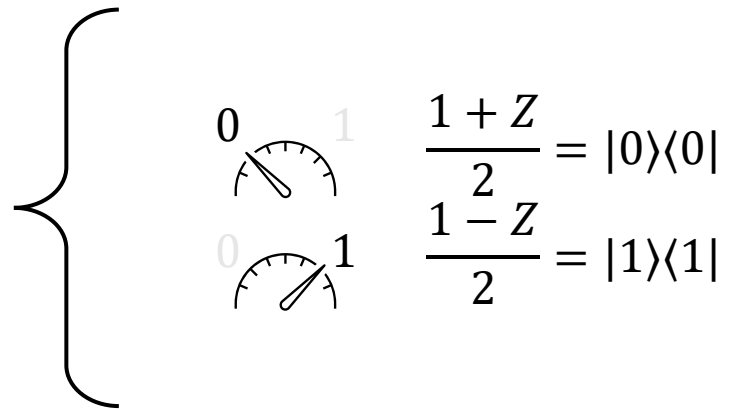
Thus

$$E_0 = \langle 0_E | U | 0_E \rangle = |0_P\rangle\langle 0_P| \quad (8.25)$$

$$E_1 = \langle 1_E | U | 0_E \rangle = |1_P\rangle\langle 1_P|, \quad (8.26)$$

and therefore

$$\mathcal{E}(\rho) = E_0 \rho E_0 + E_1 \rho E_1, \quad (8.27)$$



# Quantum Computation of Topological Invariant

- Computing a topological invariant, but now, in the language of a quantum computer.
  - Topological Dynamical Quantum Phase Transition (TDQPD)
  - In a field theory (<https://journals.aps.org/prl/abstract/10.1103/PhysRevLett.122.250401>)
  - Minimal Experimental Data (PRXQuantum.4.030323)

Dynamical Quantum Phase Transition

Skip technical encoding of problem

Fermionic topological invariants in  $(k,w)$  space

Poles in dynamical manifold of the quantum (Green's) correlation function

Diagonalization of free-theory — experiment

Take home assignment, do this for 2, 4 lattice sites (4, 8 qubits)

Calculation of topo invariant

## Quantum Computation of Dynamical Quantum Phase Transitions and Entanglement Tomography in a Lattice Gauge Theory

Niklas Mueller<sup>1,2,3,\*</sup>, Joseph A. Carolan<sup>4</sup>, Andrew Connelly<sup>5</sup>, Zohreh Davoudi<sup>1,6,†</sup>, Eugene F. Dumitrescu<sup>7,‡</sup> and Kübra Yeter-Aydeniz<sup>8</sup>

<sup>1</sup>Maryland Center for Fundamental Physics and Department of Physics, University of Maryland, College Park, Maryland 20742, USA

<sup>2</sup>Joint Quantum Institute, NIST/University of Maryland, College Park, Maryland 20742, USA

<sup>3</sup>Department of Physics, InQubator for Quantum Simulation (IQUS), University of Washington, Seattle, Washington 98195, USA

<sup>4</sup>Department of Computer Science, University of Illinois at Urbana-Champaign, Urbana, Illinois 61801, USA

<sup>5</sup>Department of Physics, North Carolina State University, Raleigh, North Carolina 27695, USA

<sup>6</sup>Joint Center for Quantum Information and Computer Science, NIST/University of Maryland, College Park, Maryland 20742, USA

<sup>7</sup>Computational Sciences and Engineering Division, Oak Ridge National Laboratory, Oak Ridge, Tennessee 37831, USA

<sup>8</sup>The MITRE Corporation, Emerging Engineering and Physical Sciences Department, 7515 Colshire Drive, McLean, Virginia 22102-7539, USA

 (Received 18 October 2022; revised 26 May 2023; accepted 21 July 2023; published 18 August 2023)

Strongly coupled gauge theories far from equilibrium may exhibit unique features that could illuminate the physics of the early universe and of hadron and ion colliders. Studying real-time phenomena has proven challenging with classical-simulation methods, but is a natural application of quantum simulation. To demonstrate this prospect, we quantum compute nonequal-time correlation functions and perform entanglement tomography of nonequilibrium states of a simple lattice gauge theory, the Schwinger model, using a trapped-ion quantum computer by IonQ Inc. As an ideal target for near-term devices, a recently predicted [Zache *et al.*, Phys. Rev. Lett. 122, 050403 (2019)] dynamical quantum phase transition in this model is studied by preparing, quenching, and tracking the subsequent nonequilibrium dynamics in three ways: (i) overlap echos signaling dynamical transitions, (ii) nonequal-time correlation functions with an underlying topological nature, and (iii) the entanglement structure of nonequilibrium states, including entanglement Hamiltonians. These results constitute the first observation of a dynamical quantum phase transition in a lattice gauge theory on a quantum computer, and are a first step toward investigating topological phenomena in nuclear and high-energy physics using quantum technologies.

## II. QUANTUM COMPUTING DYNAMICAL QUANTUM PHASE TRANSITIONS

Consider the massive lattice Schwinger model with the Hamiltonian

$$H(m) = \frac{1}{2a} \sum_{n=0}^{N-1} (\psi_n^\dagger \mathcal{U}_n \psi_{n+1} + \text{H.c.}) + m \sum_{n=0}^{N-1} (-1)^n \psi_n^\dagger \psi_n + \frac{ae^2}{2} \sum_{n=0}^{N-1} E_n^2$$

on a one-dimensional (spatial) lattice with  $N$  sites and periodic boundary conditions (PBCs), with mass  $m$ , electric coupling  $e$ , and lattice spacing  $a$ .  $\psi_n^\dagger$  and  $\psi_n$  denote creation and annihilation operators for the (staggered) fermions, respectively.  $\mathcal{U}_n$  is the link and  $E_n$  the electric field operator, satisfying the commutation relation  $[E_n, \mathcal{U}_m] = \delta_{nm} \mathcal{U}_n$ . The Hamiltonian commutes with Gauss's law operator at each site,  $G_n \equiv E_n - E_{n-1} - Q_n$ , where

$$Q_n \equiv \psi_n^\dagger \psi_n - \frac{1}{2} [1 - (-1)^n] \quad (2)$$

is the staggered fermion charge. The gauge-invariant physical Hilbert space contains states that satisfy  $G_n |\psi\rangle^{\text{phys}} = 0$ .

# Topological Dynamics

Adding a topological  $\theta$  term  $e\theta/2\pi \sum_n E_n$  to Eq. (1), and upon performing a chiral transformation to absorb the  $\theta$  parameter into a (complexified) fermion mass term, yields the Hamiltonian [183–188]

$$\begin{aligned} \tilde{H}(m, \theta) = & \sum_{n=0}^{N-1} \frac{1 - ma \sin(\theta)(-1)^n}{2a} (\psi_n^\dagger \mathcal{U}_n \psi_{n+1} + \text{H.c.}) \\ & + \sum_{n=0}^{N-1} m \cos(\theta)(-1)^n \psi_n^\dagger \psi_n + \frac{ae^2}{2} \sum_{n=0}^{N-1} E_n^2. \end{aligned} \quad (3)$$

At  $t = 0$   $m \rightarrow -m$  temporal band inversion. Winds the quantum state space. Band inversion is a typical ingredient in the generation of topological phases in condensed matter physics.

## Mapped onto a long-range interacting fermionic model. (1D Model)

Explicitly, in the purely fermionic form,  $\mathcal{U}_n$  is set to one in Eqs. (1) and (8), and the electric field term in Eq. (1) is replaced by a (translation-invariant) long-range fermionic density-density interaction [148,196]

$$\frac{ae^2}{2} \sum_{n=0}^{N-1} E_n^2 \rightarrow ae^2 \sum_{n,m=0}^{N-1} v(d_{nm}) \mathcal{Q}_n \mathcal{Q}_m \equiv H_I, \quad (11)$$

where  $d_{nm} = \min(|n - m|, N - |n - m|)$ , and

$$v(d) \equiv \frac{3 - N}{4(N - 2)} \times \begin{cases} d & \text{if } d = 0, 1 \\ d + \frac{d^2 - 3d + 2}{3 - N} & \text{if } 2 \leq d \leq \frac{N}{2} - 1. \\ \frac{N^2 - 8}{4(N - 3)} & \text{if } d = \frac{N}{2} \end{cases} \quad (12)$$

The resulting Hamiltonian reads

$$H(m) = H_0(m) + H_I, \quad (13)$$

with  $H_I$  defined above and

$$H_0 = \frac{1}{2a} \sum_{n=0}^{N-1} (\psi_n^\dagger \psi_{n+1} + \text{H.c.}) + m \sum_{n=0}^{N-1} (-1)^n \psi_n^\dagger \psi_n \quad (14)$$

being the noninteracting fermionic part of the Hamiltonian.

$$L(t) \equiv \langle \Psi(0) | \Psi(t) \rangle = \langle \text{GS}(m) | e^{-iH(-m)t} | \text{GS}(m) \rangle, \quad (5)$$

from which one can define an intensive rate function,

$$\Gamma(t) \equiv \lim_{N \rightarrow \infty} \left\{ -\frac{1}{N} \log(|L(t)|) \right\}. \quad (6)$$

The nonanalyticities of Eq. (6) correspond to DQPTs and can be extracted on lattices as small as four to eight sites with small finite-volume effects in the  $e/|m| \lesssim 1$  regime [148]. The second quantity is a set of nonequal-time correlation functions (NECFs), defined in the staggered lattice formulation as

$$g_q(t) = \sum_{j=0}^{N/2-1} e^{-i\frac{2\pi qj}{N/2}} \left[ g_j^{\text{even}}(t) + g_j^{\text{odd}}(t) \right], \quad (7)$$

where  $q \in [-(N/4), (N/4) - 1]$  and

$$g_j^{\text{even(odd)}}(t) \equiv \langle \psi_{2j(2j+1)}^\dagger(t) \mathcal{U}_{2j(2j+1),0(1)}(t) \psi_{0(1)}(0) \rangle, \quad (8)$$

with  $\langle \dots \rangle \equiv \langle \text{GS}(m) | \dots | \text{GS}(m) \rangle$  and  $\mathcal{U}_{n,m}(t) \equiv \prod_{k=m}^{n-1} \mathcal{U}_k(t)$  ( $\mathcal{U}_{n,n} = 1$ ). From  $g_q(t)$ , an integer-valued topological order parameter can be extracted [195]

$$v(t) \equiv n_-(t) - n_+(t), \quad (9)$$

where

$$n_{\pm}(t) \equiv \frac{1}{2\pi} \oint_{\mathcal{C}_{\pm}(t)} dz \tilde{g}_z^\dagger \partial_z \tilde{g}_z. \quad (10)$$

Here,  $\mathbf{z} \equiv (q, t')$ ,  $g_z \equiv g_q(t')$ , and  $\tilde{g}_z \equiv g_z/|g_z|$ . Concretely,  $\mathcal{C}_{\pm}(t)$  runs clockwise (counterclockwise) in the positive (negative) half of wave numbers  $q$  in the  $(q, t')$  plane, i.e.,  $\mathcal{C}_+(t) : (0, 0) \rightarrow (N/4 - 1, 0) \rightarrow (N/4 - 1, t) \rightarrow (0, t) \rightarrow (0, 0)$  and similarly for  $\mathcal{C}_-(t)$ . Note that  $t'$  is continuous and  $q$  is discrete, hence integral and derivative become a sum and finite difference along the  $q$  sections of  $\mathcal{C}_{\pm}(t)$ . Equation (9), which is valid at arbitrary coupling  $e$ , changes by an integer whenever the system undergoes a dynamical quantum phase transition. We refer the reader to Ref. [148] for more details, and here we focus on a quantum computational representation of the topological phenomenon.

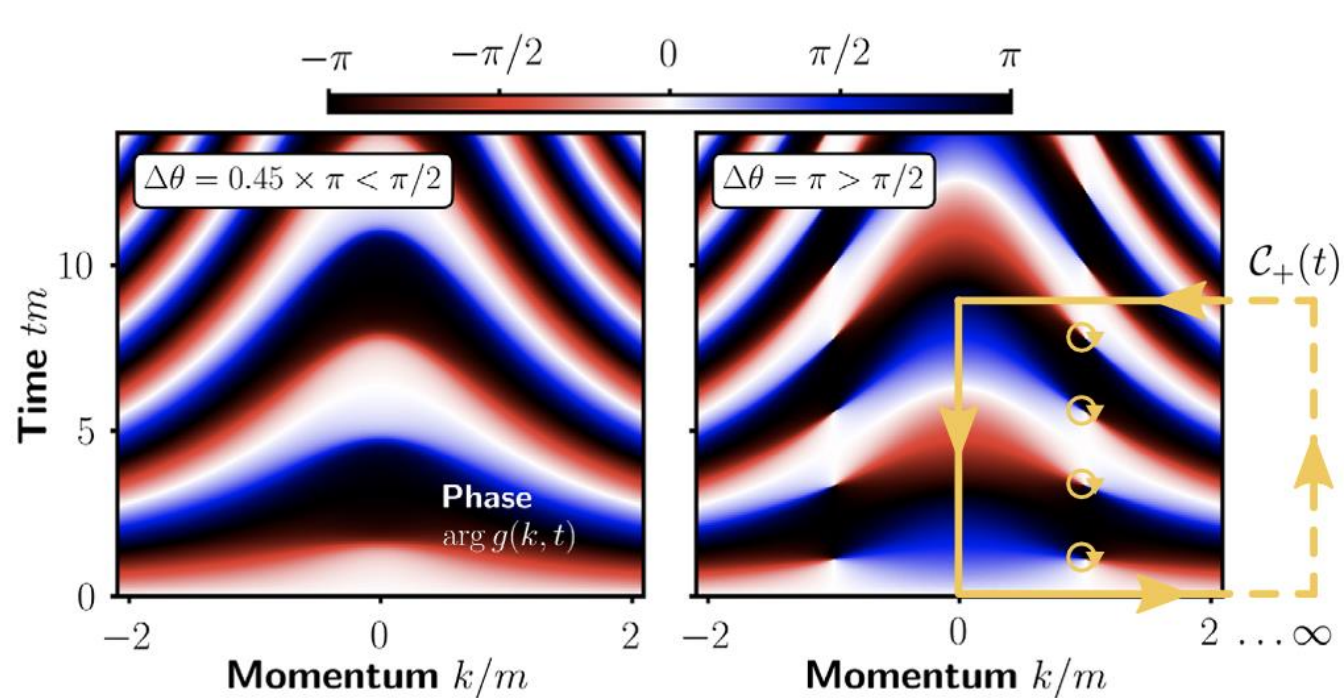


FIG. 1. Phase of the time-ordered correlator [Eq. (2)] after  $\theta$  quenches at vanishing gauge coupling. The real-time evolution of the phase exhibits qualitative differences when the quench is weaker or stronger than the critical value  $\Delta\theta_c = \pi/2$ , exemplified here for  $\Delta\theta = 0.45\pi$  (left) and  $\Delta\theta = \pi$  (right). The phase is analytic for small quenches ( $|\Delta\theta| < \Delta\theta_c$ ), while for large quenches ( $|\Delta\theta| > \Delta\theta_c$ ) vortices form at  $(\pm k_c, t_c^{(n)})$ . The integration path  $\mathcal{C}_+(t)$ , here shown for  $tm \approx 9$ , encloses a discrete number of vortices (marked by yellow circles), leading to integer increments of the topological invariant  $\nu$  as time progresses (see Fig. 2).

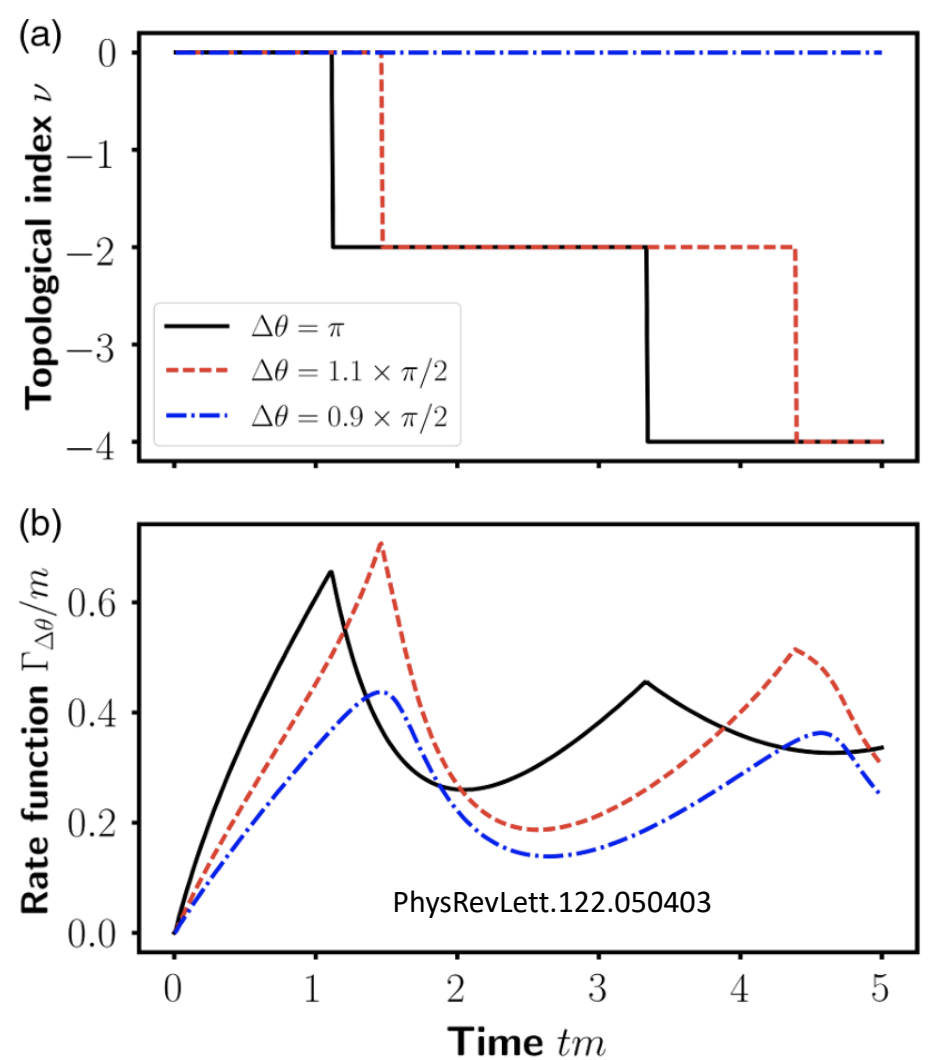


FIG. 2. Dynamical topological transitions at vanishing gauge coupling. (a) The topological invariant exhibits jumps at critical times  $t_c^{(n)} = (2n - 1)\pi/[2\omega(k_c)]$  with  $n \in \mathbb{N}$ , if  $|\Delta\theta| > \pi/2$ , while the dynamics is topologically trivial for  $|\Delta\theta| < \pi/2$ . (b) For  $|\Delta\theta| > \pi/2$ , the rate function [Eq. (5)] shows nonanalytic kinks at times  $t_c^{(n)}$ .

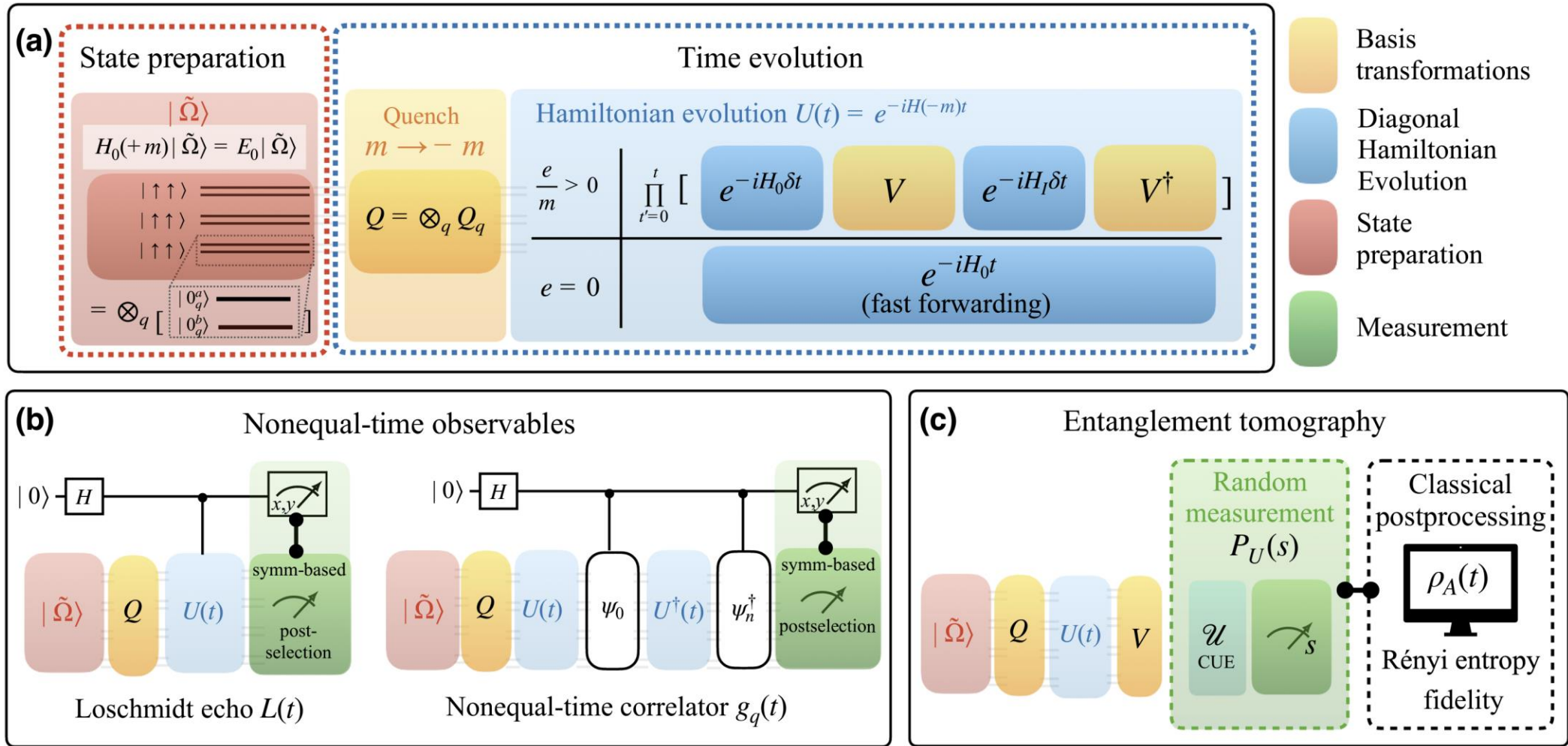


FIG. 1. (a) Implementation strategy to prepare ground state of the noninteracting Schwinger model and simulate nonequal-time evolution after a quantum quench, involving basis changes  $V$  from position to momentum space. Free ( $H_0$ ) and interacting ( $H_I$ ) parts of the time evolution are performed in a diagonal basis. The quench from  $m$  to  $-m$  is achieved via a basis transformation from the vacuum of the free theory in momentum-space computational basis with mass  $m$  to that with mass  $-m$ . (b) Interferometry schemes, employed to compute Loschmidt echo  $L(t)$  [Eq. (5)] and NECFs  $g_q(t)$  [Eq. (7)], include a symmetry-based error-mitigation scheme. (c) Entanglement tomography scheme to extract Rényi entropies, fidelities, as well as the reduced density matrix  $\rho_A(t)$  from an entanglement Hamiltonian ansatz that is constrained by a classical optimization based on a number of random measurements.

# Experimental Data

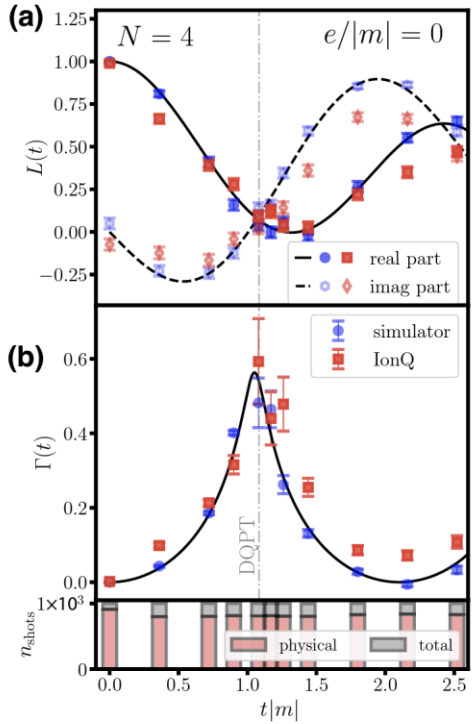


FIG. 2. (a) Real (solid line, dark-colored symbols) and imaginary (dashed line, light-colored symbols) parts of the Loschmidt echo  $L(t)$  from an ideal simulator (blue circles) versus error-mitigated results from IonQ Harmony (red squares), for  $N = 4$  sites,  $e = 0$  and  $|m|a = 0.9$ . (b) Rate function  $\Gamma(t)$  reconstructed from the same data. The bottom panels show the number of shots resulting in a physical, i.e., occupation-number symmetry-preserving result (red bars) versus all results (gray bars).

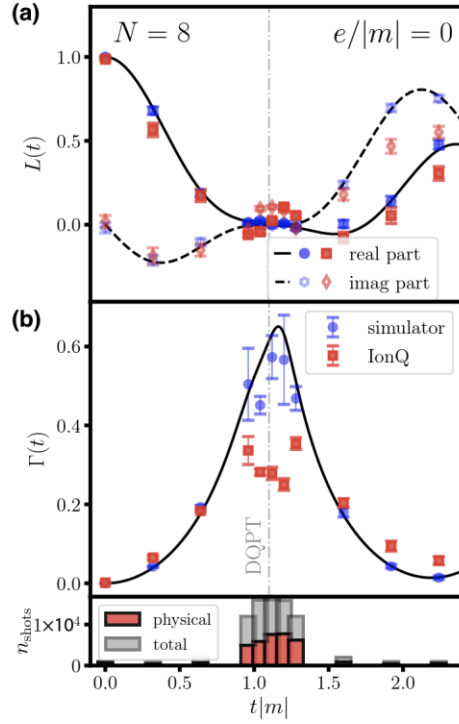


FIG. 3. (a) Real (solid line, dark-colored symbols) and imaginary (dashed line, light-colored symbols) parts of the Loschmidt echo  $L(t)$  from an ideal simulator (blue circles) versus error-mitigated results from IonQ Harmony (red squares), for  $N = 8$  sites,  $e = 0$  and  $|m|a = 0.8$ . (b) Rate function  $\Gamma(t)$  reconstructed from the same data. The bottom panels shows the number of shots resulting in a physical, i.e., occupation-number symmetry-preserving result (red bars) versus all results (gray bars).

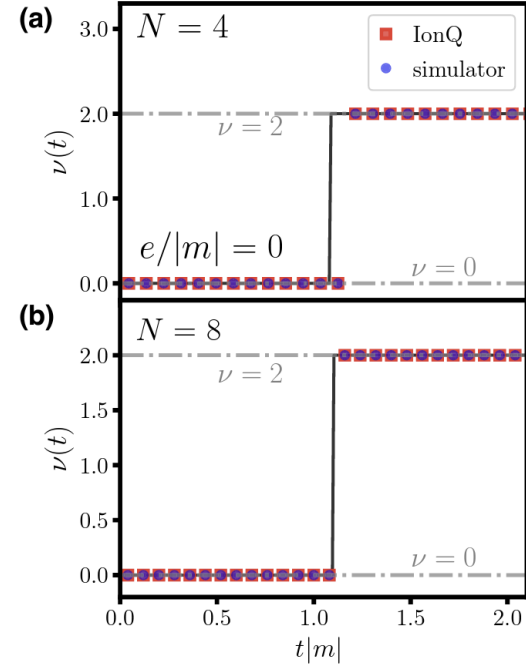


FIG. 7. Topological index  $\nu(t)$ , computed via Eqs. (9) and (10) from  $g_q(t)$  (Fig. 6), for (a)  $N = 4$ ,  $|m|a = 0.9$ , and (b)  $N = 8$ ,  $|m|a = 0.8$ . Exact results are black lines, simulator results are blue symbols, and IonQ results are red symbols. Horizontal dotted-dashed gray lines indicate the possible integer values  $\nu(t)$  can take.

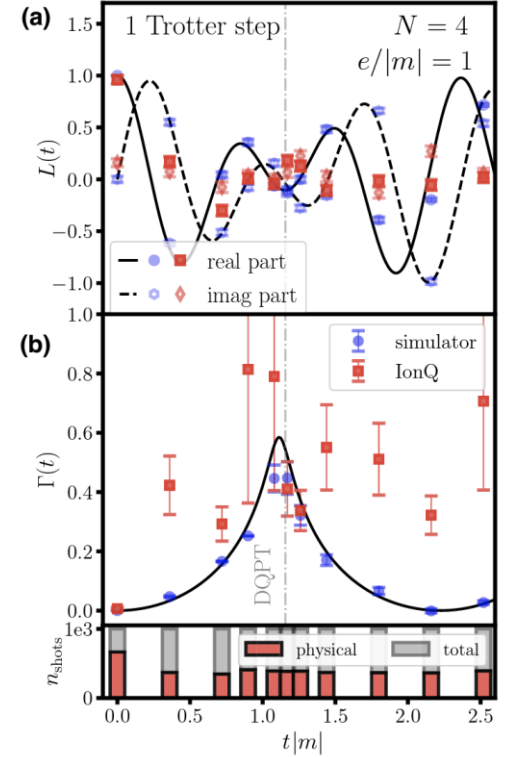


FIG. 5. (a) Loschmidt echo  $L(t)$  from an ideal simulator (blue) versus error-mitigated results from IonQ Harmony (red), for  $N = 4$  sites,  $|m|a = 0.9$  at finite coupling  $e/|m| = 1$ , using a one step Trotter scheme. (b) Rate function  $\Gamma(t)$ , with bottom panels showing physical (red), i.e., occupation-number symmetry respecting results, versus all results (gray).

### III. ENTANGLEMENT TOMOGRAPHY

Entanglement structure and state fidelity of nonequilibrium states can be obtained following Refs. [159,163–165, 168], based on random measurement. Our circuit-based approach is summarized in Fig. 1(c). One can compute Rényi entropies and fidelities, and reconstruct the reduced density matrix using a generalization of the Bisognano-Wichmann (BW) theorem [179,180]. The second-order bipartite Rényi entropy is

$$S_A^{(2)}(t) \equiv -\log_2\{\text{Tr}_A(\rho_A^2(t))\}, \quad (22)$$

The reduced density matrix  $\rho_A(t)$  of system  $A$  is reconstructed using the entanglement Hamiltonian tomography (EHT) protocol of Ref. [168], based on the BW theorem [179,180] generalized to nonequilibrium states. To do so,  $\rho_A(t)$  is parametrized as [209]

$$\rho_A(t) = e^{-H_A(t)}, \quad (25)$$

in terms of an entanglement Hamiltonian (EH),

$$H_A(t) \equiv H_A(t; \{\beta_i, \mu_i\}) = \sum_{j \in A} \beta_j(t) H_j + \sum_{j \in A} \mu_j(t) T_j. \quad (26)$$

Inspired by the BW theorem,  $H_j$  are the local operators in Eq. (13) (“energy densities”) and  $T_i$  are commutators of the latter. In practice, at  $e = 0$ , these are

$$\begin{aligned} H_j &= \{(-1)^n \psi_n^\dagger \psi_n, \psi_n^\dagger \psi_{n+1} + \text{H.c.}\}, \\ T_j &= \{i(\psi_n^\dagger \psi_{n+1} - \text{H.c.}), \psi_n^\dagger \psi_{n+2} + \text{H.c.}\}, \end{aligned} \quad (27)$$

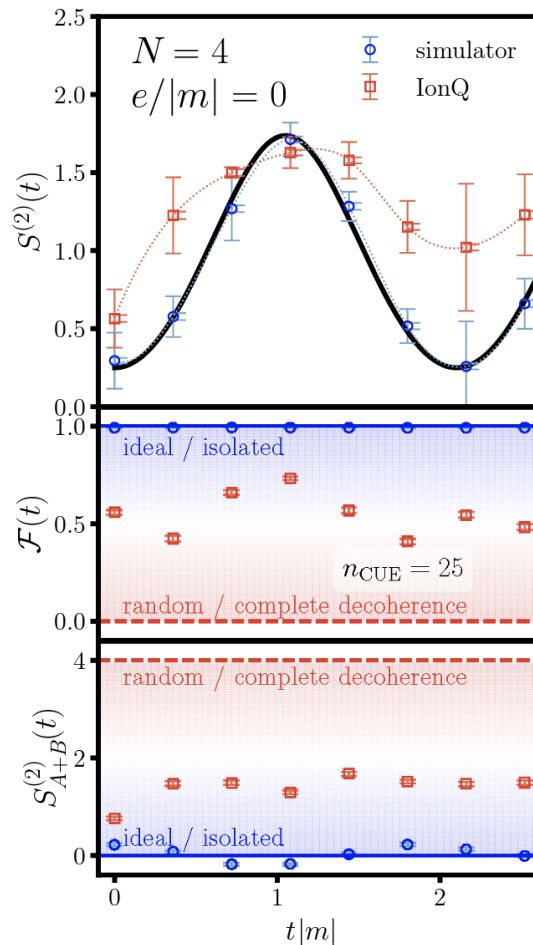


FIG. 8. The top panel shows Rényi entropy averaged over subsystems  $A$  and  $B$ ,  $S^{(2)}(t) \equiv (1/2)(S_A^{(2)}(t) + S_B^{(2)}(t))$  [with  $S_A^{(2)}$  and similarly  $S_B^{(2)}$  defined in Eq. (22)], for  $N = 4$ ,  $|m|a = 0.9$ ,  $e = 0$ ,  $n_{\text{CUE}} = 25$ , and  $n_{\text{shots}} = 1000$ , including simulator (blue symbols) and IonQ (red symbols) results. The middle panel depicts fidelity  $\mathcal{F}(t)$  [Eq. (23)]. The bottom panel shows the Rényi entropy of the full system,  $S_{A+B}^{(2)}$  (relative to the environment). Blue horizontal lines in the middle and bottom panels indicate ideal results, and a horizontal red line indicates zero fidelity or maximal entropy ( $\rho(t) = \mathbb{I}/2^N$ ), respectively.

### APPENDIX G: FURTHER RESULTS ON ENTANGLEMENT TOMOGRAPHY

The results of the entanglement tomography analysis for the largest system with  $N = 8$  lattice sites are presented in this Appendix. The significant gate count, as evident from

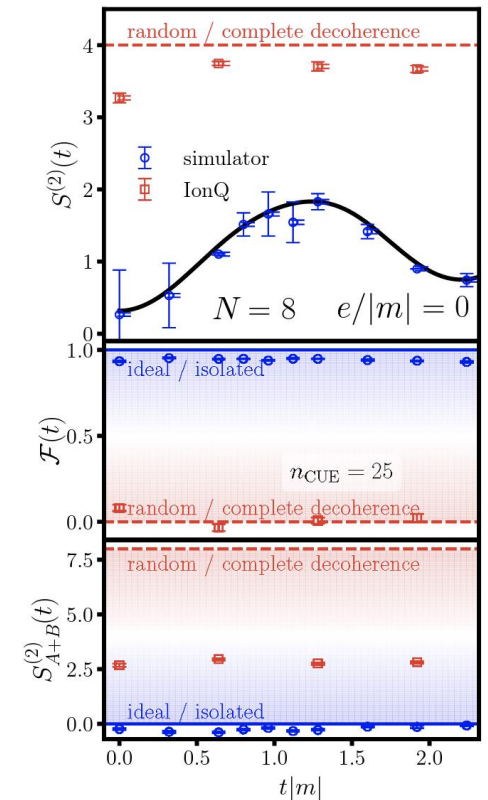


FIG. 18. The top panel shows Rényi entropy averaged over subsystems  $A$  and  $B$ ,  $S^{(2)}(t) \equiv (1/2)(S_A^{(2)}(t) + S_B^{(2)}(t))$  [with  $S_A^{(2)}$  and similarly  $S_B^{(2)}$  defined in Eq. (22)], for  $N = 8$ ,  $|m|a = 0.8$ ,  $e = 0$ ,  $n_{\text{CUE}} = 25$ , and  $n_{\text{shots}} = 1000$ , including simulator (blue symbols) and IonQ (red symbols) results. The middle panel depicts fidelity  $\mathcal{F}(t)$  [Eq. (23)]. The bottom panel shows the Rényi entropy of the full system,  $S_{A+B}^{(2)}$  (relative to the environment). Blue horizontal lines in the middle and bottom panels indicate ideal results, a horizontal red line indicates zero fidelity or maximal entropy ( $\rho(t) = \mathbb{I}/2^N$ ), respectively. See Fig. 19 for a close up of the lower two panels.

# Summary

- Examined topological features of topological quantum error correcting code families:
  - A topological field theory underpinning discrete-logic
  - Emergent quasiparticles in the laboratory
- Topologies of logical computations
  - Unitary maps (real time evolution)
    - Eigenstates are fixed points and sources of curl for differential flow field
  - Measurement and imaginary time evolution
    - Measurement settings are
- Algorithms to compute dynamical & topological phase transition in a quantum field theory.